Chapter 23

Current Status of Mid-Infrared Semiconductor-Laser-based Sensor Technologies for Trace-Gas Sensing Applications

Rafał Lewicki and Mohammad Jahjah
Electrical & Computer Engineering Department, Rice University, Houston, Texas, USA

Yufei Ma
Electrical & Computer Engineering Department, Rice University, Houston, Texas, USA and National Key Laboratory of Science and Technology on Tunable Lasers, Harbin Institute of Technology, Harbin, China

Przemysław Stefański and Jan Tarka
Electrical & Computer Engineering Department, Rice University, Houston, Texas, USA and Laser and Fiber Electronics, Institute of Telecommunications & Acoustics, Wroclaw University of Technology, Wroclaw, Poland

Manijeh Razeghi
Center for Quantum Devices, Department of EECS, Northwestern University, Evanston, Illinois, USA

Frank K. Tittel
Electrical & Computer Engineering Department, Rice University, Houston, Texas, USA

23.1 Introduction

The development of highly sensitive and selective optical sensor systems using tunable semiconductor-laser-based spectroscopic trace gas detection techniques is reported in this chapter. The quantitative detection and monitoring of trace gas molecules in real-world applications such as atmospheric chemistry, pollution monitoring, and industrial process control in most cases require the targeting of fundamental vibrational–rotational (V-T) molecular absorption bands located between the 3- and 24-μm wavelengths. The mid-infrared fundamental absorption bands of several small molecules of potential interest for trace gas monitoring are shown in Fig. 23.1 within two mid-infrared atmospheric transmission windows. The upper panel shows absorption spectra in the atmospheric window between the bending fundamental of water centered at around 1600 cm^{-1} and the water OH stretches starting above 3200 cm^{-1}. The lower panel shows absorption spectra in the atmospheric window below the water bending fundamental. The logarithmic ordinate scales are the integrated intensities of the lines on a per-molecule basis. These spectral regions can be covered by narrow-linewidth and high-performance semiconductor lasers in particular quantum cascade lasers (QCLs)[1–2] and interband cascade lasers ICLs.[3–4] Therefore, trace gas optical spectroscopic sensors using a QCL or ICL as an excitation source are responsible for improving the spectral resolution of the measurements and achieving real time, continuous ultrasensitive detection of trace gas molecular species at the concentration levels from the percent level down to parts per trillion (ppt).

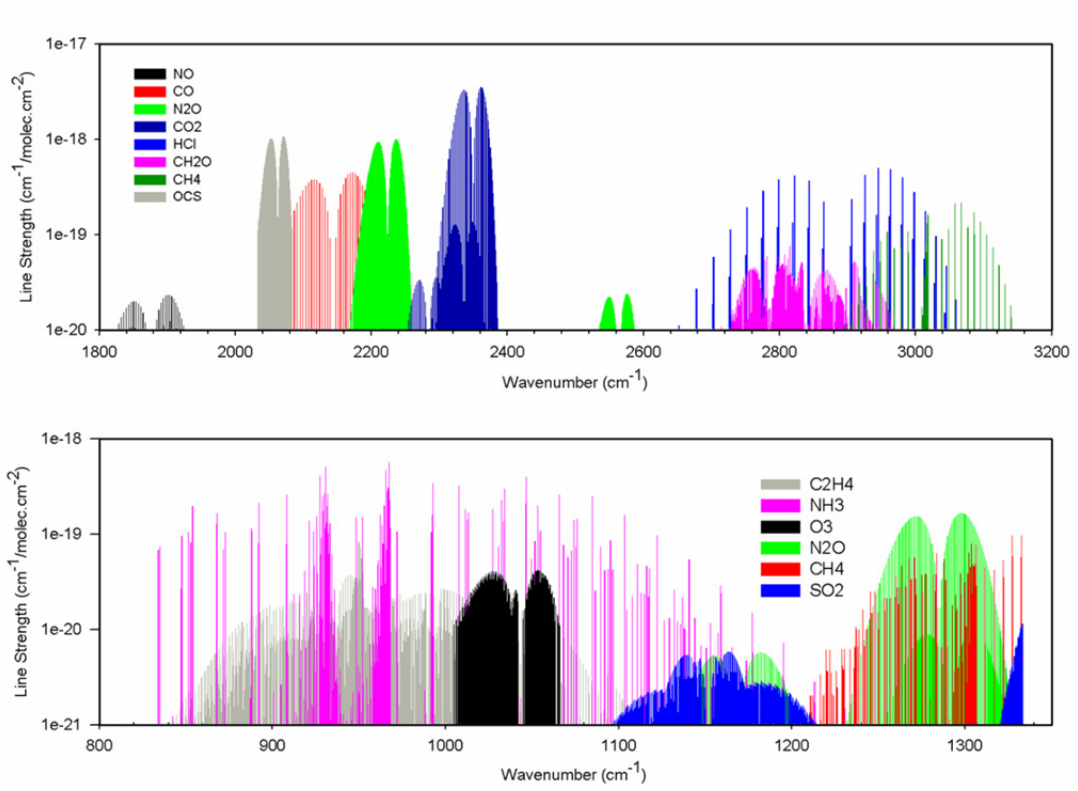

Figure 23.1 High-resolution simulated molecular absorption spectra within two mid-infrared atmospheric transmission windows (reprinted from Ref. 14).

In this chapter the spectroscopic detection and monitoring of various specific molecular species, such as ethane (C_2H_6),[5] methane (CH_4),[6–7] nitrous oxide (N_2O), ammonia (NH_3),[8–9] nitric oxide (NO),[9,10] carbon monoxide (CO),[11] and sulfur dioxide (SO_2)[12] is described. All of these molecules were detected based on three different detection techniques: tunable diode laser absorption spectroscopy (TDLAS), conventional photoacoustic spectroscopy (CPAS), and quartz-enhanced photoacoustic spectroscopy (QEPAS).[13–16] Other ultrasensitive and highly selective spectroscopic techniques that are employed by research groups for trace gas detection include: balanced detection,[17] laser-induced breakdown spectroscopy (LIBS),[18,19] noise immune cavity enhanced optical heterodyne molecular spectroscopy (NICE-OHMS),[20,21] Faraday rotation spectroscopy (FRS),[22–24] and frequency comb spectroscopy.[25,26] These spectroscopic techniques can achieve minimum detectable absorption losses in the range from 10^{-8} to 10^{-11} $cm^{-1}/\sqrt{Hz}$. The choice of an optimum detection technique depends on the requirements of the specific application and the characteristic features of the single-mode-operated infrared laser source such as available optical power, tunable wavelength, or beam quality. Moreover, to perform gas detection measurements, various parameters such as gas pressure and modulation depth also need to be optimized.

The conventional method to perform sensitive laser-based absorption spectroscopy measurements is to increase optical path length by using an optical multipass gas cell. The most common absorption spectroscopy for quantitative measurements of gas species is TDLS. In this chapter this technique together with 2*f* wavelength modulation spectroscopy (WMS) was used for detecting C_2H_6, which is of interest in atmospheric chemistry, oil and gas prospecting,[27] and in medical breath analysis.[28] Moreover, C_2H_6 is a greenhouse gas, and the variation of its concentration in the atmosphere, mainly due to fossil fuel and biofuel consumption, biomass burning process, and natural gas loss, can lead to long-term climate changes.[29] To monitor C_2H_6 concentration levels, a spectroscopic trace-gas sensor based on a 3.36-µm continuous-wave (CW), thermoelectrically cooled (TEC), distributed-feedback (DFB) laser diode was developed to access one of the optimal absorption lines of C_2H_6 in the mid-infrared region. TDLAS was performed with an ultracompact 57.6-m effective optical path length innovative spherical multipass cell capable of 459 passes between two mirrors separated by 12.5 cm and with a sensor control board used as a driver controller for the DFB diode laser and the photodetector. This trace-gas sensor technology will be evaluated as an *in situ* sensor system for landfill applications.

To detect environmental concentration levels of NH_3,[8] a spectroscopic trace-gas sensor based on a 10.4-µm CW external-cavity quantum cascade laser (EC-QCL) using a conventional CPAS technique was employed. CPAS is a powerful and well-established indirect spectroscopic technique based on the photoacoustic effect, where an acoustic wave is created as a result of the absorption of modulated radiation by molecular species. When it propagates within resonant photoacoustic cells, the acoustic wave can be detected either by a single sensitive microphone[30,31] or an array of microphones to achieve more-sensitive results for trace-gas detection.[32] Therefore, in the CPAS technique, no photodetector is required. For the purpose of monitoring the QCL power, an infrared detector or optical power meter located directly behind after the photoacoustic cell is usually employed. In order to obtain an optimal acoustic signal value, the laser modulation frequency is typically selected to match the first longitudinal acoustic resonance of the photoacoustic cell, given by the equation $f = v/2L$, where v is the speed of sound, and L is the length of the cell. The overall photoacoustic cell dimensions, including sound isolation and buffer gas volumes, are typically ~10 cm or more, which might be considered large for some applications, especially when employed with small- sized QCLs. In most cases, the

resonance frequencies of the photoacoustic cells are above 1 kHz, insulating the CPAS experiment from low-frequency environmental noise.[33–35] The detected photoacoustic signal S_{PA} is described by the following equation: $S_{PA} = CP\alpha cM$, where C is the photoacoustic cell constant in Pa/(Wcm^{-1}), P is optical power of the laser in W, α is the absorption coefficient of the targeted gas in cm^{-1}/(molecule cm^{-3}), c is concentration in molecule/cm^3, and M is the response of the microphone in V/Pa.

For quantitative measurements of CH_4 and N_2O, SO_2, NO, and CO, different CW room-temperature (RT) DFB QCL sources emitting at 7.83, 7.24, 5.26 and 4.6 μm were employed, respectively. As a detection technique, a novel approach to the photoacoustic detection of trace gases, utilizing a quartz tuning fork (QTF) as an acoustic transducer, was employed. This technique, named quartz-enhanced photoacoustic spectroscopy (QEPAS), was first reported by our Rice University Laser Science Group in 2002.[13,36] The key innovation of QEPAS is to invert the common CPAS approach and accumulate the acoustic energy in a sharply resonant piezoelectric QTF with a very high quality Q factor of > 10,000, rather than in a broadband microphone with a low-Q-factor (~ 200) resonant CPAS gas cell. Due to the very narrow QTF resonance curve, QEPAS possesses high immunity to environmental acoustic noise. Moreover, small dimensions of the QTF allow performance of sensitive trace gas concentration measurements using an ultrasmall acoustic detection module (ADM), where the total volume of the analyzed gas sample is < 4 mm^3.[37]

A readily available QTF that is well suited for QEPAS applications is commonly used in digital clocks and watches as frequency standards and has a resonance frequency at 32,768 Hz in vacuum. The QTF is able to detect weak acoustic waves generated when the modulated optical radiation interacts with a trace gas. The mechanical deformation of the QTF due to interaction with the acoustic waves results in the generation of electrical charges on its electrode pairs. The electrical charges can be measured as either a current or voltage by the electrodes that are connected to an ultralow-noise preamplifier and lock-in detection electronics. An enhancement of the QEPAS signal can be achieved when two metallic tubes acting as a microresonator (mR) are added to the QTF sensor architecture. A typical configuration, used in most reported QEPAS-based gas sensors where the QTF is positioned between the mR tubes to probe the acoustic waves excited in the gas contained inside the mR, can be found in Refs. 10, 16, 36, 38, and 39. Other QEPAS configurations, such as off-beam QEPAS, are also possible.[40,41] Furthermore, two novel modifications of the QEPAS sensor architecture based on interferometric photoacoustic spectroscopy[42] and resonant opto-thermoacoustic detection[43] were recently reported.

A recent optimization study of the geometrical mR parameters showed that the highest QEPAS signal-to-noise ratio (SNR) is achieved for two 4.4-mm-long and 0.5- to 0.6-mm-inner-diameter tubes.[39] However, for a typical QCL beam, short mR tubes with a larger inner diameter are advantageous in facilitating the optical alignment of the QCL excitation beam with the respect to the mR and the QTF. Therefore, to simplify the optical alignment process and eliminate any potential optical fringes, the 4-mm-long tubes with 0.84-mm inner diameter are commonly used for QEPAS experiments in the mid-infrared region. A direct, side-by side comparison of a QEPAS sensor using a QTF and a CPAS sensor based on a state-of-the-art differential resonance photoacoustic cell was demonstrated in Ref. 40.

23.2 Tunable Diode Laser Absorption Spectroscopy (TDLAS) for Ethane Detection

A TDLAS trace-gas sensor based on a 3.36-μm CW, TEC, DFB laser diode from nanoplus GmbH was developed.[5,44,45] An optimum interference-free C_2H_6 absorption line located at

2976.8 cm^{-1} was selected as the optimum target wavelength. TDLAS was performed with an ultracompact multipass gas absorption cell with an effective optical path length of 57.6 m. In addition, a compact state-of-the-art surface-mounted electronic control board and data acquisition module was used for the first time in order to replace bulky and costly laboratory instrumentation. A noise equivalent concentration (NEC) of 130 pptv (1σ) in dry nitrogen for a 1-s lock-in time constant was achieved at a pressure of 200 Torr, due to low electrical and optical noise, and the high sensitivity of the TEC mercury-cadmium-telluride (MCT) detector (Vigo System S.A. PVI-4TE-4).

23.2.1 Laser characterization

The experimentally determined DFB laser diode light intensity and voltage as a function of injected current (LIV) curves are presented in Fig. 23.2(a). The laser diode's temperature and current tuning characteristics are shown in Fig. 23.2(b). Experimentally determined and based on Fig. 23.2(b), the DFB laser diode current and temperature tuning coefficients are –0.022 cm^{-1}/mA and –0.26 cm^{-1}/ºC, respectively.

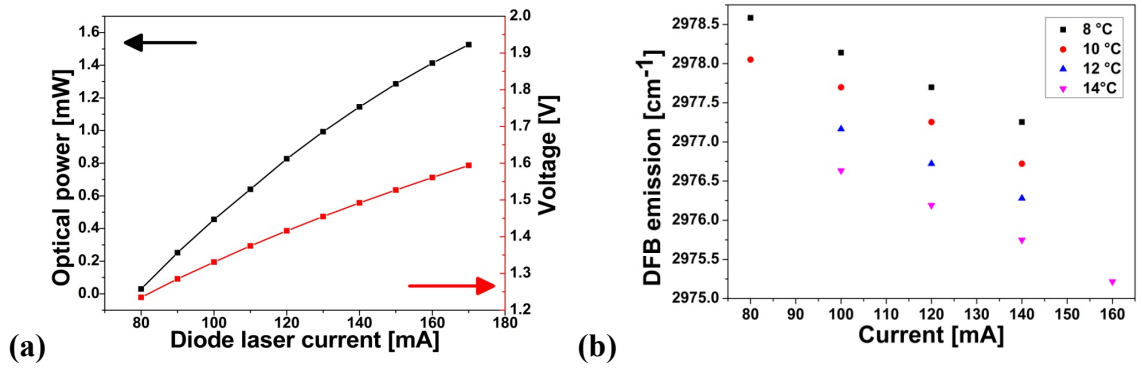

Figure 23.2 (a) Light intensity versus current and voltage (LIV) curves for a 3.36-µm CW, TEC, DFB laser diode operating at 10 °C. (b) Temperature and current tuning characteristics of the laser diode (reprinted from Ref. 5).

23.2.2 Optical sensor architecture

The C_2H_6 optical sensor, depicted in Fig. 23.3, uses a 3.36-µm CW, TEC GaInAsSb/AlGaInAsSb DFB laser diode as a spectroscopic source to target the optimum C_2H_6 absorption line located at 2976.8 cm^{-1}. The DFB laser diode is packaged in a TO5 can. Its output beam is collimated by a Black Diamond™ aspheric lens (CL) (Thorlabs, model C036TME-E) and focused by a second lens (L), using a 200-mm focal length planoconvex CaF_2 lens (Thorlabs LA5714-E), into the input entrance hole of a novel multipass gas absorption cell (MC) (Sentinel Photonics, Monmouth Junction, NJ), based on a modified spherical Herriott MC concept.

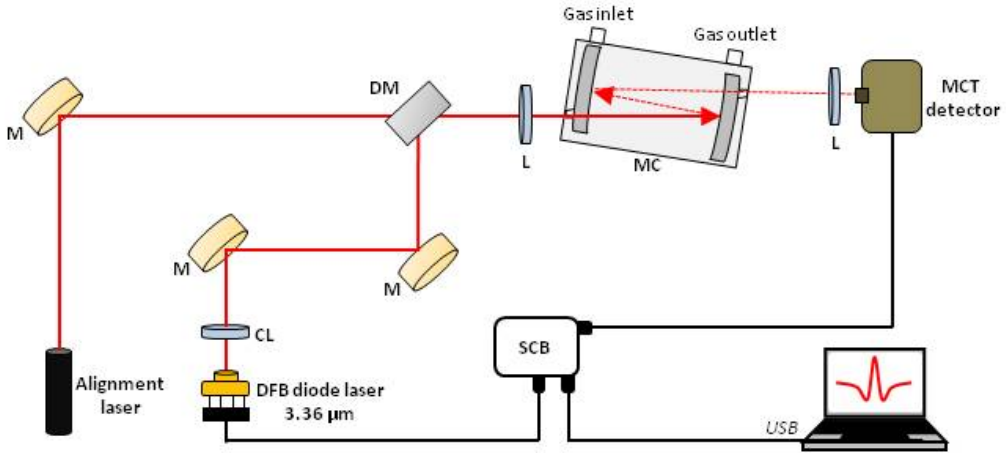

Figure 23.3 Schematic of a C_2H_6 gas sensor using a 3.36-µm DFB laser diode as an excitation source. M – mirror, CL – collimating lens, DM – dichroic mirror, MC – multipass cell, L – lens, SCB – sensor control board.

Furthermore, an ultracompact state-of-the-art surface-mounted electronic control board and data acquisition module control electronics provided by Sentinel Photonics, denoted as the sensor control board (SCB) in Fig. 23.3, was used to provide the diode laser current and temperature control as well as data processing capability, replacing traditional laboratory instrumentation such as two lock-in amplifiers and a function generator. The TEC of the MCT detector is also connected to the SCB for signal data acquisition. A photograph of the SCB, the multipass cell, and the MCT detector are depicted in Fig. 23.4(a). Alignment of the optical sensor was realized by adding a visible semiconductor laser diode (λ = 630 nm). This beam was combined with the beam from the 3.36-µm DFB diode laser by using a dichroic mirror (DM) (ISO Optics, model BSP-DI-25-3). The processing unit used for the SCB is based on a TI MSP430. The laser diode temperature and TEC are controlled by thermistor sensing and the power output, respectively. In addition, the SCB provides laser diode current drive and modulation. The SCB dimensions are 70 mm × 50 mm × 10 mm. During wavelength modulation performance, the data is synchronously sampled via an embedded analog-to-digital converter, and characteristic absorption spectra are produced by a digital lock-in amplifier algorithm. The SCB can also synchronously apply a continuous saw-tooth current ramping at 8 Hz, which is the 32-bit lock-in amplifier signal. Therefore, the total control and acquisition systems power consumption to generate wavelength-modulated ramp spectra is < 0.4 W.

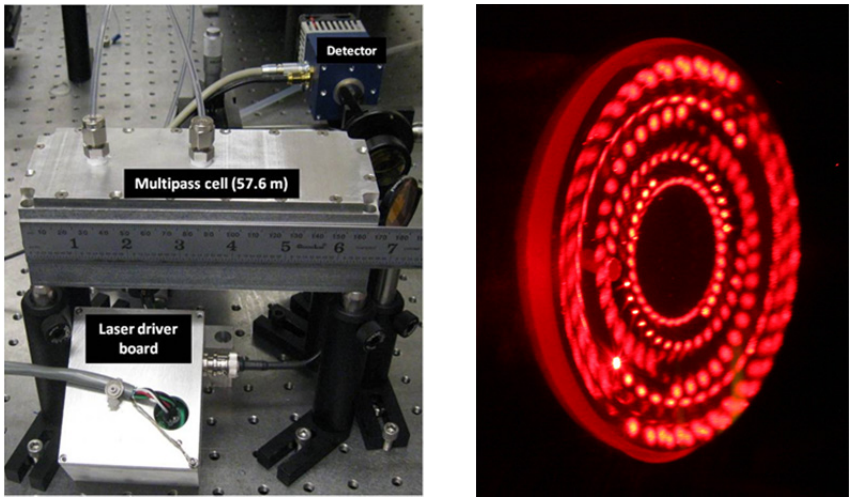

(a) (b)

Figure 23.4 (a) Photograph of an innovative long-path, small-volume multipass gas cell (MC dimensions: 17 × 6.5 × 5.5 cm; distance between MC mirrors: 12.5 cm; effective optical path length: 57.6 m with 459 passes) with novel compact surface-mounted control electronics from Sentinel Photonics. (b) Spot pattern of a modified spherical Herriott MC (from Sentinel Photonics website).

The novel ultracompact multipass cell is formed by two dielectric-coated spherical glass substrates. The reflectivity provided by these substrates exceeds 99.5%. Based on the spherical Herriott cell concept,[46,47] with two coaxial spherical mirrors and with a distance of 12.5 cm between the mirrors providing a minimal spot overlap to reduce etalon fringe effects, 459 laser beam passes are created inside the multipass cell, resulting in an effective optical path length of 57.6 m. The spot pattern is shown in Fig. 23.4(b).

23.2.3 Experiments and results

The targeted C_2H_6 absorption line located at 2976.8 cm^{-1} is detected by setting the laser diode temperature and injected current to 9.5 °C and 136.7 mA, respectively. Wavelength scanning across the C_2H_6 absorption line is performed with 8 Hz of continuous saw-tooth current ramping provided by the SCB. In addition, a sinusoidal modulation of 16 KHz is superimposed on the ramping signal with amplitude of 15.6 mA. These parameters are required for the 2*f* WMS detection technique. A vacuum pump is connected to the multipass cell in order to operate at a cell pressure of 200 Torr. The multipass cell was filled with a calibrated mixture of 100 ppbv C_2H_6 in nitrogen (N_2) (ppbv is parts per billion by volume). The 2*f* signal of 100 ppbv C_2H_6 and the baseline (which is determined after filling the multipass cell with pure N_2 at a pressure of 200 Torr) are presented in Fig. 23.5(a).

A low-noise C_2H_6 sensor baseline was achieved by using a single driver module for laser diode and data acquisition. A SNR of 770 was obtained, yielding an NEC of 130 pptv (1 σ) for a 1-s sample averaging time.

To assess the performance of the TDLAS-WMS sensor for the detection of C_2H_6, we studied its linearity by plotting the 2*f* amplitude signal as measured by a lock-in detection as a function of the calibrated concentration of ethane in the multipass gas cell (at 5-, 10-, 15-, 25-,

50- and 100-ppbv concentration levels). Gas dilution was realized by using a commercial gas mixer (Gas Dilution System series 4040) from Environics. Figure 23.5(b) depicts the response of the C_2H_6 sensor versus concentration fitted with a linear slope.

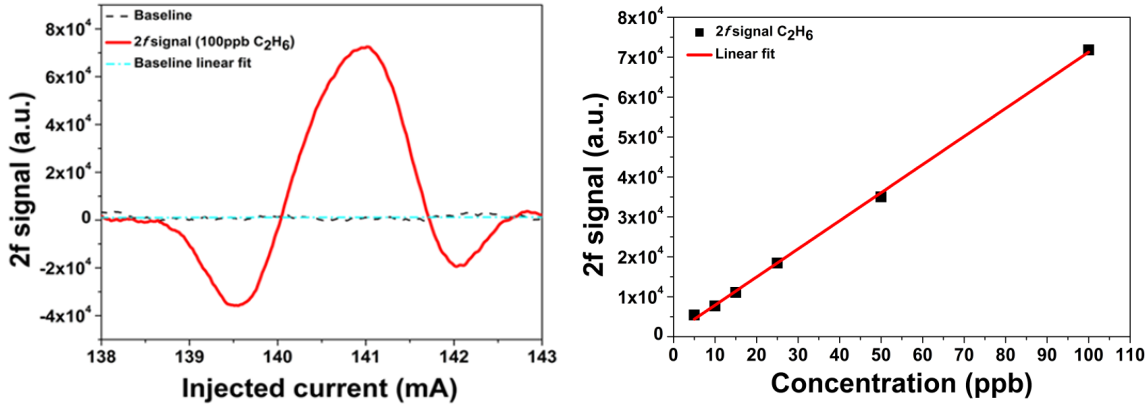

Figure 23.5 (a) 2*f* WMS signal for a C_2H_6 line at 2976.8 cm^{-1} at 200 Torr obtained with compact multipass gas cell. (b) 2*f* WMS amplitude signal as function of C_2H_6 concentration.

23.3 Environmental Detection of Ammonia using an EC-QCL-based C-PAS Sensor Platform

In order to improve the current understanding of the dynamics of ammonia in industrial/urban and rural areas, continuous long-term measurements of atmospheric NH_3 were conducted in Houston and at a Texas Commission on Environmental Quality (TCEQ) sampling site in a remote area of Dallas/Fort Worth, respectively. Ammonia (NH_3) is normally present in the atmosphere at trace concentration levels and, like other nitrogen-containing trace gases such as N_2O, NO, NO_2 and HNO_3, plays a significant role in atmospheric chemistry. The emission of NH_3 to the atmosphere is primarily caused by anthropogenic sources such as animal waste, poultry, mineral fertilizers, or biomass burning but also by natural sources such as animals, oceans, vegetation, and the decomposition of plants.[48] Moreover, for highly developed urban areas, an additional increase of atmospheric ammonia concentration levels can be observed due to industrial and automobile/truck traffic activities.

From a perspective of environmental concern, NH_3 is a precursor of particulate matter (PM) due to its chemical reaction with sulfuric and nitric acid to produce different ammonium salts: ammonium sulfate [$(NH_4)_2SO_4$], ammonium nitrate (NH_4NO_3), or ammonium bisulfate (NH_4HSO_4). As a result, the abundance of NH_3 in the atmosphere has a considerable impact on aerosol nucleation and composition. Despite the importance of ammonia in atmospheric chemistry, the National Ambient Air Quality Standards by the United States Environmental Protection Agency (US EPA) currently does not regulate NH_3, and there is limited knowledge about NH_3 concentration levels in the atmosphere.

23.3.1 Sensor configuration and results

Environmental detection of ammonia concentration levels was performed with a 10.4-µm EC-QCL-based sensor platform employing an amplitude-modulated photoacoustic spectroscopy

(AM-PAS) technique [see Fig. 23.6(a)]. A TEC CW EC-QCL system from Daylight Solutions (Model 21106-MHF) can be tuned from 933 to 1006 cm^{-1}, emitting a maximum optical power of 64 mW. Coarse, single-mode frequency tuning can be performed with minimum step resolution of 0.01 cm^{-1} by simply rotating the diffraction grating. For high-resolution spectroscopy, a sinusoidal voltage, with a maximum amplitude of 100 V, can be applied to the piezoelement, enabling a mode-hop-free piezoscan within ~ 1 cm^{-1}. Within the EC-QCL spectral tuning range, the NH_3 absorption line in the ν_2 fundamental absorption band of ammonia at 965.35 cm^{-1} is targeted. This absorption line is optimal for atmospheric NH_3 detection in terms of absorption coefficient, laser power, and the absence of potential interfering species such as CO_2 and H_2O. The laser beam is modulated by a mechanical chopper at 1.8 kHz, and a 9.1-cm-long differential resonant photoacoustic cell is used as the state-of-the-art photoacoustic detector.[49] In a differential photoacoustic cell, two identical cylindrical channels, connected to each other at both ends, are equipped with an electret microphone, which is placed in the middle of each channel, where the maximum pressure oscillations are located. The signal from each microphone is delivered to the differential amplifier and then analyzed by an external lock-in amplifier. In order to achieve detection of NH_3 at single-ppb concentration levels, which is required for sensitive atmospheric measurements, the optical beam is passed through the cell three times. A pyroelectric detector placed directly behind after a 10-cm reference cell, filled with 0.2% of NH_3 at 30 Torr, was used for frequency locking as well as for monitoring the available EC-QCL output power.

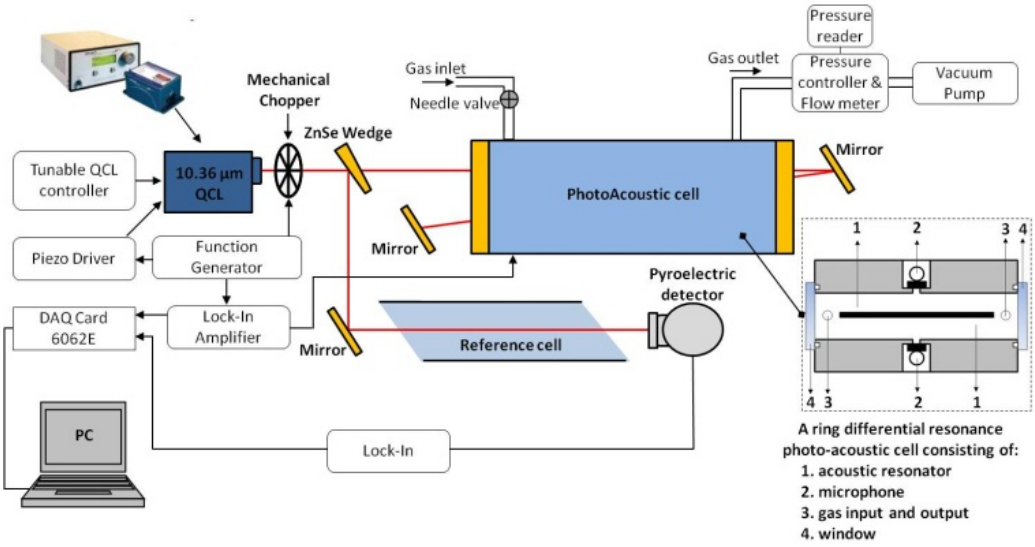

(a)

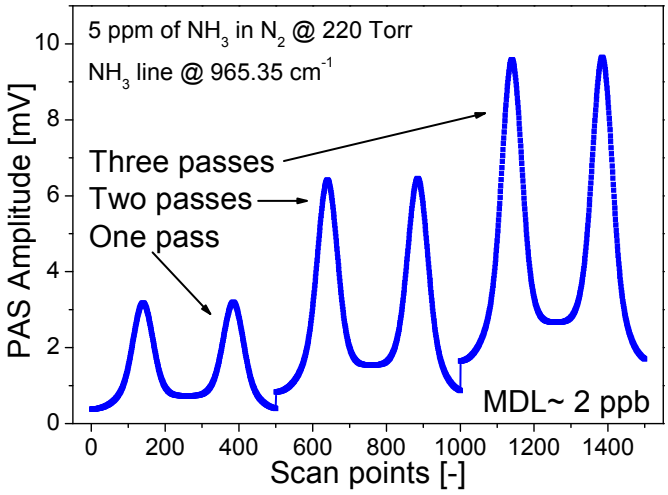

(b)

Figure 23.6 (a) Mid-infrared AM-PAS-based sensor platform for NH_3 atmospheric detection. (b) AM-PAS signal for reference mixture of 5-ppm NH_3 in N_2 after one, two, and three laser beam passes through the photoacoustic cell.

The pressure inside the system was kept at 220 Torr, while the flow was maintained at 150 ml/min. In order to minimize the ammonia adsorption to surfaces and to prevent water vapor condensation in the sensor, the sensor enclosure was heated to 38 °C. The minimum detectable concentration of ammonia for the sensor, when the laser beam passes three times through the photoacoustic cell, was ~ 2 ppbv for a 5-s data acquisition time [see Fig. 23.6(b)]. After averaging the data for 100 s, a sub-ppbv NH_3 concentration level of ~ 0.7 ppbv was achieved.

The AM-PAS-based NH_3 sensor platform was deployed at the University of Houston North Moody Tower monitoring site during three different seasons (winter 2010, summer/fall 2011, winter 2011) and at the continuous ambient monitoring station (CAMS) 75 monitoring site in the Fort Worth/Dallas area (between May 30, 2011 and June 30, 2011) as part of the summer 2011 TCEQ campaign. The 2010/2011 results of environmental ammonia measurements are reported in Ref. 8. The NH_3 sensor platform was again deployed on top of the University of Houston North Moody Tower during the 2012 summer months in order to investigate the correlations between NH_3 and particle number concentrations (PNCs) [measured by a condensation particle counter (CPC)] and to compare NH_3 concentration levels over the same period of last year. Monitoring PNC alongside NH_3 levels and incorporating meteorological parameters as well as other air pollutants data measured by a TCEQ CAMS allows us to investigate the effect of NH_3 on local and regional air quality with respect to PM formation.

A time series of atmospheric NH_3 concentration and particle number concentration levels for city of Houston, TX, measured between July 19, 2012 and July 31, 2012 is depicted in Fig. 23.7. The emission sources that were identified as being responsible for some of the elevated concentration levels in the Greater Houston urban area are: the W. A. Parish electric power plant and the Houston Ship Channel. In general, the high NH_3 concentration levels observed during this period were expected due to the more-intense ammonia evaporation from natural sources (soil, vegetation, decomposition of plants) and agricultural (animal waste, mineral fertilizer, pesticides). In addition, high ambient temperatures observed during the summer significantly improve the conversion of ammonia from the particle phase to gas phase.

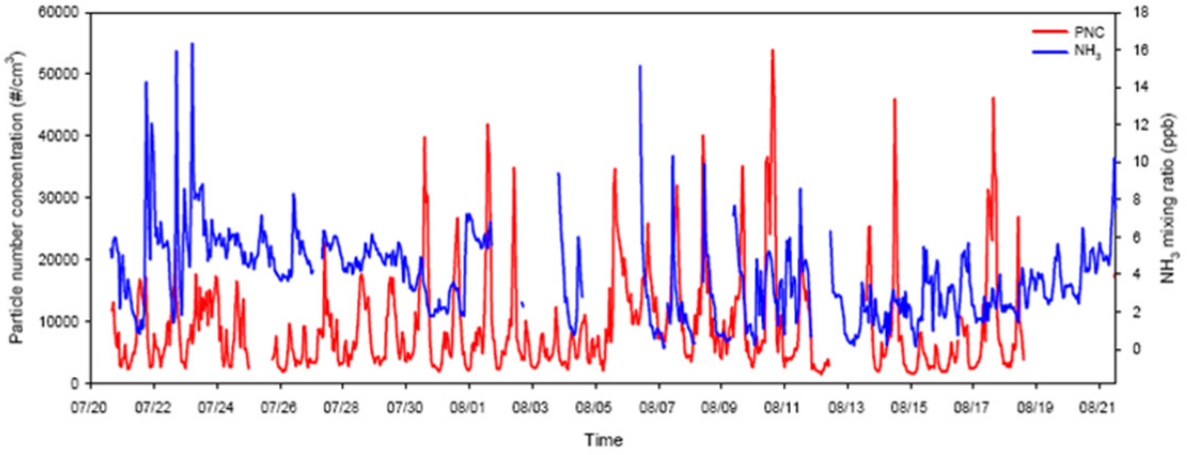

Figure 23.7 Time series of atmospheric NH_3 concentration and particle number concentration levels for Houston, TX, measured from July 20 to August 21, 2012.

23.4 Quartz-Enhanced Photoacoustic Spectroscopy (QEPAS)

23.4.1 Methane and nitrous oxide detection

23.4.1.1 7.83-µm DFB-QCL for methane and nitrous oxide detection

A 7.83-µm DFB-QCL operating in a CW regime and mounted inside a high-heat-load (HHL) package with high emitted optical power (~ 300 mW at 15 °C) from Adtech Optics was used to detect CH_4 and N_2O. Inside the HHL package, an aspheric lens was placed in front of the QCL in order to collimate the emitted beam. The HHL package is sealed by the ZnSe window that transmits ~ 95% of the initial QCL optical power. The QCL output power as well as the current and temperature tuning curves are shown in Figs. 23.8(a) and (b), respectively.

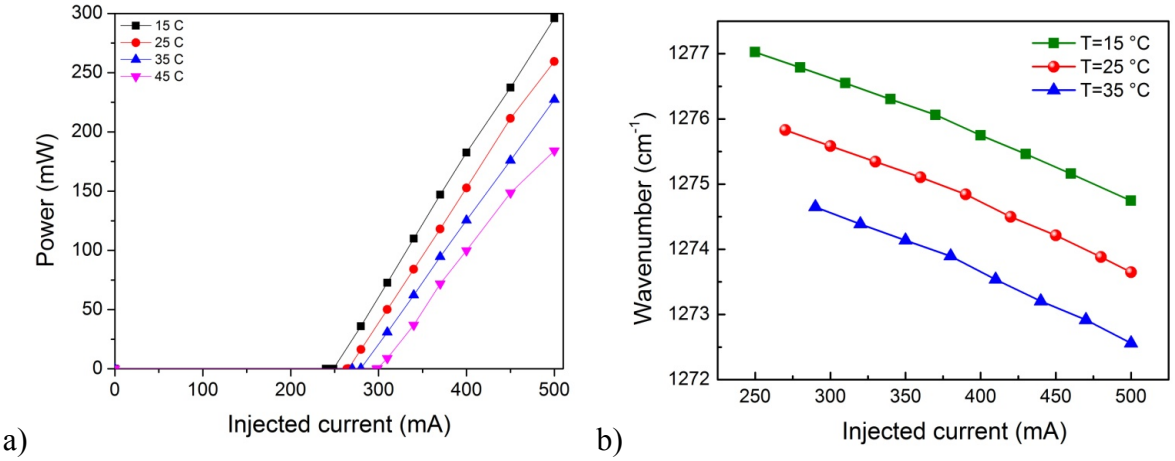

Figure 23.8 (a) Measured optical power for Adtech Optics 7.83-µm CW DFB QCL operating at 15, 25, 35, and 45 °C. (b) Temperature and current properties.

Tuning coefficients for the DFB-QCL current and temperature changes were experimentally determined to be –0.01 cm^{-1}/mA and –0.01 cm^{-1}/°C, respectively. A wide temperature range can be used with this DFB-QCL from 15 to 60 °C. Therefore, an important wavenumber range, from 1273 to 1277 cm^{-1}, can be covered with this QCL. In this mid-infrared spectral range, CH_4 and N_2O absorption lines are accessible.

23.4.1.2 Experiments and results

In order to detect the CH_4 and N_2O absorption lines that are accessible within the 7.83-µm AdTech Optics DFB-QCL tuning range, the QCL operating temperature was fixed at 21.5 °C and the injection current was varied between 430 and 500 mA. With the available output power of > 120 mW from this QCL a 2*f* WMS signal for N_2O and CH_4 in ambient laboratory air is detected. In order to determine the optimum measurement conditions such as the optical modulation depth and the CH_4 and N_2O gas pressure, a detailed evaluation of the QEPAS system was performed.

Figure 23.9 depicts the 2*f* QEPAS signals for N_2O and CH_4 in ambient laboratory air (blue plot) and for a calibrated mixture of 1.8-ppmv N_2O in N_2 (red plot). Both measurements were recorded at a total gas pressure of 100 Torr.

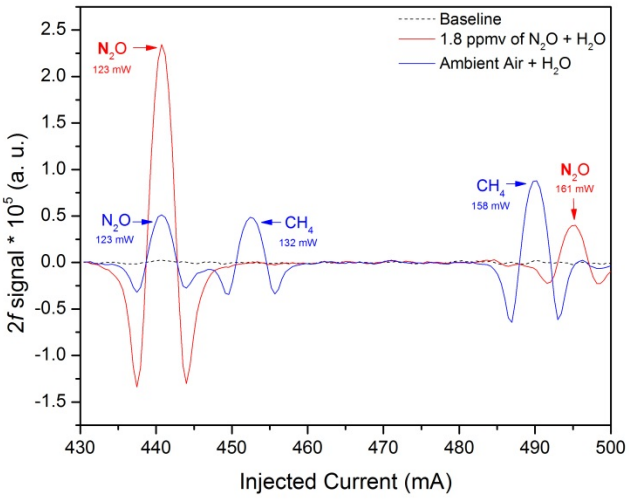

Figure 23.9 2*f* QEPAS signals for a moisturized 1.8-ppmv mixture of N_2O in N_2 (red plot) and for CH_4 and N_2O in ambient laboratory air (blue plot); the dotted curve represents the optical sensor baseline. Total gas pressure for both scans was P = 100 Torr.

Additional enhancement of the QEPAS signal amplitude was achieved by the addition of water vapor, which is an efficient accelerator for V-T relaxation processes in the gas phase. For the targeted N_2O absorption line located at 1275.5 cm^{-1}, the laboratory air N_2O concentration was calculated to be 393 ppbv based on the two N_2O QEPAS measurements shown in Fig. 23.9. The minimum detectable concentration (MDC) of the currently developed QEPAS system for CH_4 and N_2O detection is 7 ppbv and 20 ppbv, respectively, for a 1-s data acquisition time. The obtained MDC values allow performance of long-term and sensitive environmental

measurements of CH_4 and N_2O because their natural abundance in the atmosphere is at a constant level of 1.8 ppmv and 320 ppbv, respectively.

Our next goal is to implement a line-locking procedure for CH_4 and N_2O detection. Moreover, we plan to transfer the current QEPAS optical platform from a standard laboratory optical table to a custom compact optical platform (see Fig. 23.10). During this procedure, overall dimensions of the QEPAS sensor will be optimized in order to achieve a compact and transportable sensor system for CH_4 and N_2O and detection at 1275.5 cm^{-1} and 1275.041 cm^{-1}, respectively.

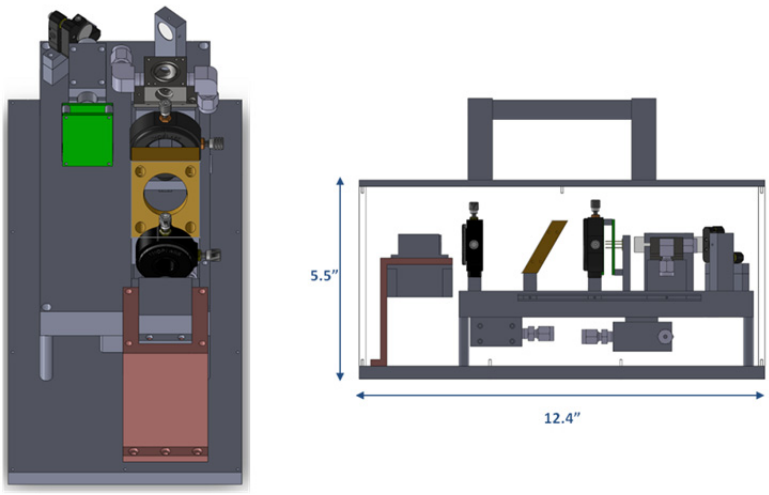

(a) (b)

Figure 23.10 (a) Front view and (b) side view of the portable compact sensor for CH_4 and N_2O detection.

23.4.2 Environmental detection of nitric oxide

The capability of detecting and quantifying nitric oxide (NO) at ppbv concentration levels has an important impact in diverse fields of applications including environmental monitoring, industrial process control, and medical diagnostics. The major sources of NO emission into the atmosphere are associated with industrial combustion processes as well as automobile, truck, aircraft, and marine transport emissions. Long term, continuous, and reliable NO concentration measurements in ambient air are important because of the role of NO in the depletion of the earth's ozone layer and in the formation of acid rain and smog.[50] Furthermore, NO is associated with numerous physiological processes in the human body and, particularly, it can be used as a noninvasive exhaled breath analyzer[51] for asthma and inflammatory lung diseases such as chronic obstructive pulmonary disease.[52]

A schematic of the developed NO QEPAS-based sensor enclosed in an aluminum enclosure is depicted in Fig. 23.11(a). A CW Maxion Technologies DFB-QCL, tunable between 1897 and 1903 cm^{-1}, was employed to target the 1900.08-cm^{-1} (5.26-μm) NO doublet absorption line of the NO fundamental band. The HHL-packaged DFB-QCL emitted ~ 100-mW optical power at an operating temperature and current of 22 °C and 890 mA, respectively. A photograph of a compact, autonomous QCL-based WMS QEPAS NO platform enclosed in a 12.3 × 5.3 × 5.1 in. aluminum enclosure is shown in Fig. 23.11(b). For sensitive NO concentration measurements, a 2*f* wavelength-modulation (WM) technique was used. A DFB-QCL current and temperature were set and controlled by a custom-made control electronics unit (CEU), which is also

employed to modulate the laser current, to lock the laser frequency to the selected absorption line, and to measure the current generated by the QTF in response to the photoacoustic signal.

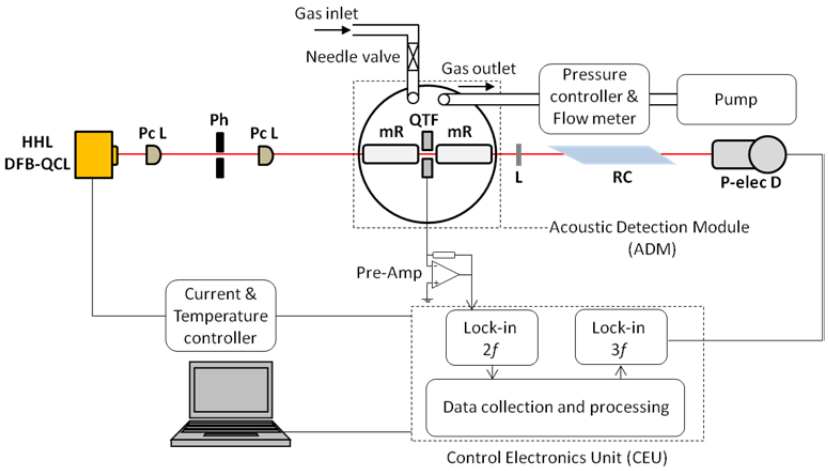

(a)

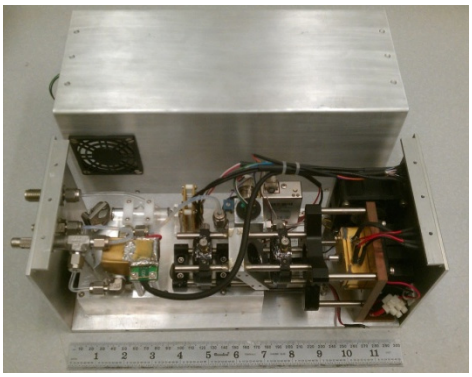

(b)

Figure 23.11 (a) Schematic and (b) completed design of a compact, RT, CW, DFB-QCL-based NO sensor platform. Pc L – plano-convex lens, Ph – pinhole, QTF – quartz tuning fork, mR – acoustic microresonator, RC – reference cell.

In order to improve the quality of the QCL beam, two plano-convex CaF_2 lenses (40-mm and 25-mm focal length) and a 300-μm pinhole are used as a spatial filter. The second lens is used to direct the laser radiation through the mR and between the prongs of QTF mounted inside the ADM with a transmission efficiency of 98%. The QCL beam exiting from the ADM is directed to a 5-cm-long reference cell, filled with a 0.11% NO in N_2 mixture at 175 Torr and a pyroelectric detector (InfraTec, LIE-332*f*-63). The 3*f* pyroelectric detector signal with a zero crossing point at the maximum of the 2*f* WM QEPAS signal was used as the reference signal for line locking of the QCL frequency to the center of the selected NO absorption line. All of the measurements were performed at a gas pressure of 250 Torr, which, according to previous experimental results, is within the optimal pressure range for QEPAS-based NO detection.[10]

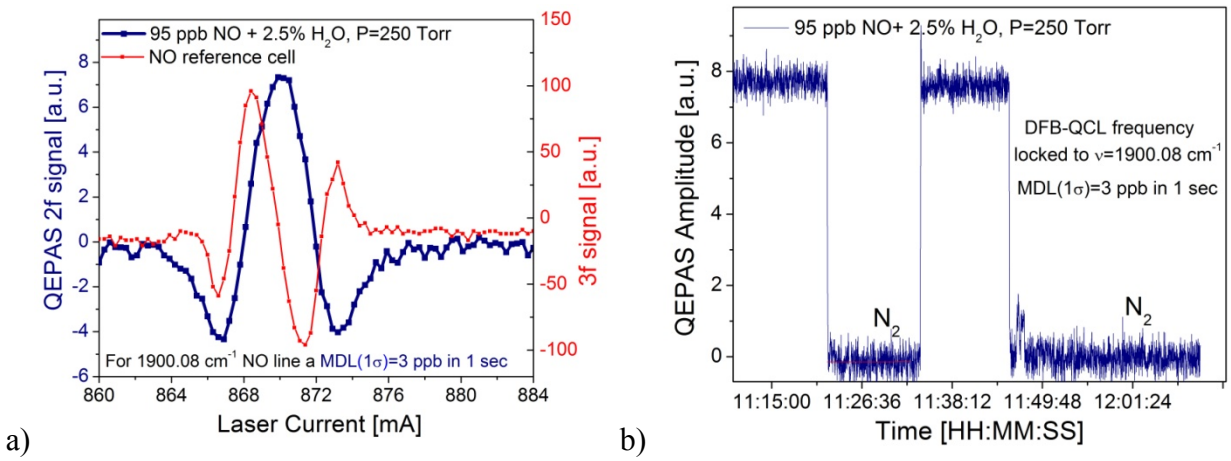

Figure 23.12 (a) 2*f* QEPAS signal amplitude when QCL frequency is tuned across and (b) locked to the NO doublet absorption line at 1900.08 cm^{-1}.

The 2*f* QEPAS signal when the DFB-QCL frequency is tuned across and locked to the H_2O and CO_2 interference-free NO doublet absorption line at 1900.08 cm^{-1} is depicted in Figs. 23.12(a) and 12(b), respectively. For a 95-ppb NO in N_2 calibrated mixture and 2.5% water vapor concentration, the calculated noise-equivalent (1 σ) concentration of NO with a 1-s averaging time is 3 ppbv at gas pressure of 250 Torr. The corresponding absorption coefficient normalized to the detection bandwidth and optical power is 6.2×10^{-9} $cm^{-1}W/\ Hz^{1/2}$.

To investigate the long-term stability of the NO sensor platform, an Allan variance analysis was performed while an ultrapure nitrogen was flushed through the ADM cell. A graph of the Allan deviation, defined as the square root of the Allan variance, is depicted in Fig. 23.13(a). This plot shows that the measurement accuracy improves with averaging time, since random noise sources can be effectively removed by the averaging process. For the completed NO QEPAS sensor, the optimum averaging time is 200 s, which corresponds to an improved NO MDC of ~ 0.3 ppbv [red line of Fig. 23.13(a)]. For the purpose of environmental monitoring, where sensor time response is not a critical parameter, a 200-s averaging time can be normally utilized to allow a detection limit of NO below 1 ppbv.

NO atmospheric data with different averaging times are illustrated in Fig. 23.13(b). During this measurement, a number of sharp peaks of NO concentration, primarily related to automobile activity, were detected. With detection sensitivity of single-ppb concentration levels this compact, a portable NO QEPAS sensor is suitable for applications in environmental monitoring, industrial processing, and medical diagnostics of human diseases.

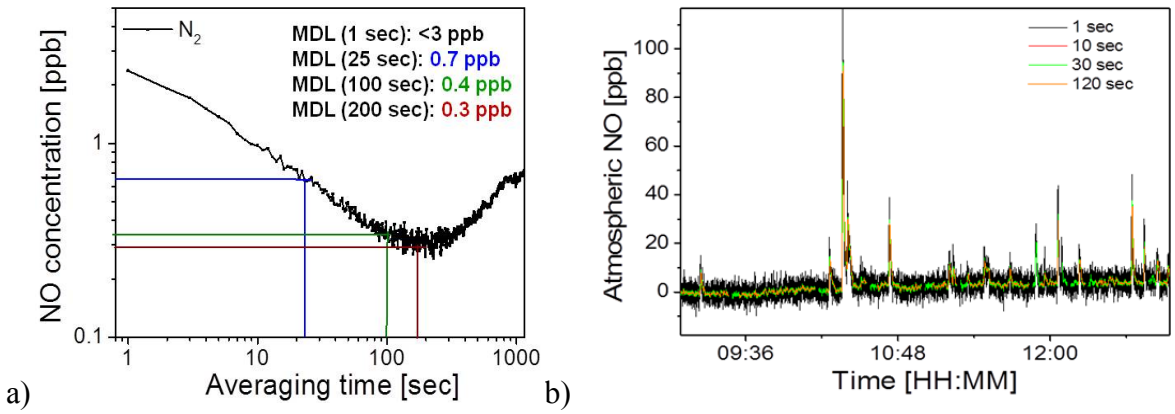

Figure 23.13 (a) Allan deviation calculated for a period during which ultrapure nitrogen was flushed through the NO QEPAS sensor system. Blue, green, and red lines show the improved NO sensitivity after 25, 100, and 200 s of the averaging time. (b) NO atmospheric data for different averaging times.

23.4.3 QEPAS-based ppb-level detection of carbon monoxide and nitrous oxide

An ultrasensitive and selective sensor based on the quartz-enhanced photoacoustic spectroscopy (QEPAS) technique was developed for monitoring atmospheric carbon monoxide (CO). CO, one of the major air pollutants in the United States, is mainly produced and released into the atmosphere by a variety of incomplete combustion activities, including the burning of natural gas, fossil fuel, and other carbon-containing fuels. CO has an important impact on atmospheric chemistry through its reaction with hydroxyl (OH) for troposphere ozone formation and also can affect the concentration level of greenhouse gases (e.g., CH_4).[1,2] Furthermore, CO, even at low concentration levels, is dangerous to human life and therefore must be accurately and precisely monitored in real time. Nitrous oxide (N_2O) on the other hand is one of the most important anthropogenic greenhouse gases that has a global warming potential of ~ 280 times greater than carbon dioxide (CO_2).[3] N_2O is mainly produced by human-related sources such as agricultural soil management, nitric acid production, as well as by emissions from automobile, truck, and aircraft from combustion of fossil fuels. It can be also produced naturally from a wide variety of biological sources present in soil and water.[4]

23.4.3.1 CW DFB-QCL-based QEPAS sensor system for CO and N_2O

The QEPAS sensor platform for atmospheric detection of CO and N_2O concentration levels is similar to the schematic in Fig. 23.11(a). The excitation source was a 4.61-μm, high-power, CW, DFB-QCL from Northwestern University,[18,19] operating at 10 ºC. An external water cooling system was used to remove the heat dissipation from the hot surface of a TEC mounted in a commercial QCL housing (ILX Lightwave Model LDM-4872). The DFB-QCL beam was collimated using a black-diamond antireflection (AR)-coated (3–5 μm) aspheric lens with a 1.7-mm effective focal length (Lightpath model 390037-IR3). Similar to the NO QEPAS system described in Section 4.2, this sensor configuration consists of two additional 50-mm and 40-mm focal length planoconvex CaF_2 lenses, and a 200-μm diameter pinhole to further improve the QCL beam quality and to pass the laser beam through the mR and the gap between the prongs of the QTF, with a transmission efficiency of > 93%. A ZnSe-wedged window acting as a beam splitter (BS) was placed after the ADM to reflect ~ 20% of the DFB-QCL beam into the

reference channel. The transmitted CW DFB-QCL beam can be monitored by an optical power meter and used for alignment verification of the QEPAS system. The laser beam, after passing through a reference cell, is detected by a pyroelectric detector (InfraTec model LIE-332*f*-63). The 3*f* reference channel signal is employed for locking of the QCL laser frequency to the peak of the CO absorption line. For precise and accurate CO-concentration measurements, a 5-cm-long reference cell filled with a 500-ppm CO:N_2 mixture at 150 Torr pressure (fabricated by Wavelength References, Inc) was used. For N_2O detection, a 10-cm-long reference cell filled with 2% N_2O in N_2 at a pressure of 100 Torr was employed. Moreover, to improve the CO and N_2O V-T relaxation processes, an external humidifier was added at the inlet to the QEPAS system. In this case the addition of a 2.6% H_2O vapor concentration to the target trace gas mixture acts as an effective catalyst that results in a higher detected amplitude for CO and N_2O QEPAS signals. A needle valve and flow meter (Brandt Instruments, Inc., Type 520) were used to set and monitor the gas flow through the QEPAS sensor system at a constant rate of 140 ml/min. A pressure controller (MKS Instruments, Inc., Type 649) and a vacuum pump were employed to control and maintain the pressure in the system. The DFB-QCL current and temperature were set and controlled by an ILX Lightwave current source (model LDX 3220) and a Wavelength Electronics temperature controller (model MPT10000), respectively.

For sensitive CO and N_2O concentration measurements, WMS with second-harmonic detection[53,54] was utilized. Modulation of the laser current was performed by applying a sinusoidal dither to the direct current ramp of the DFB-QCL at half of the QTF resonance frequency ($f = f_0/2 \sim 16.3$ kHz). The piezoelectric signal generated by the QTF was detected by a low-noise transimpedance amplifier with a 10-MΩ feedback resistor and converted into a voltage. Subsequently, this voltage was transferred to a custom-built CEU.

The optical power emitted by the DFB-QCL operating at 1250-mA current and 10 °C temperature is 987 mW in the CW operating mode [see Fig. 23.14(a)]. The experimentally determined temperature and current tuning coefficients are –0.16 cm^{-1}/°C and –0.0065 cm^{-1}/mA, respectively. This DFB-QCL can be current tuned to target the R(5) and R(6) absorption lines of the ν_1 CO fundamental band at 2165.6 cm^{-1} and 2169.2 cm^{-1}, respectively [see Fig. 23.14(b)].

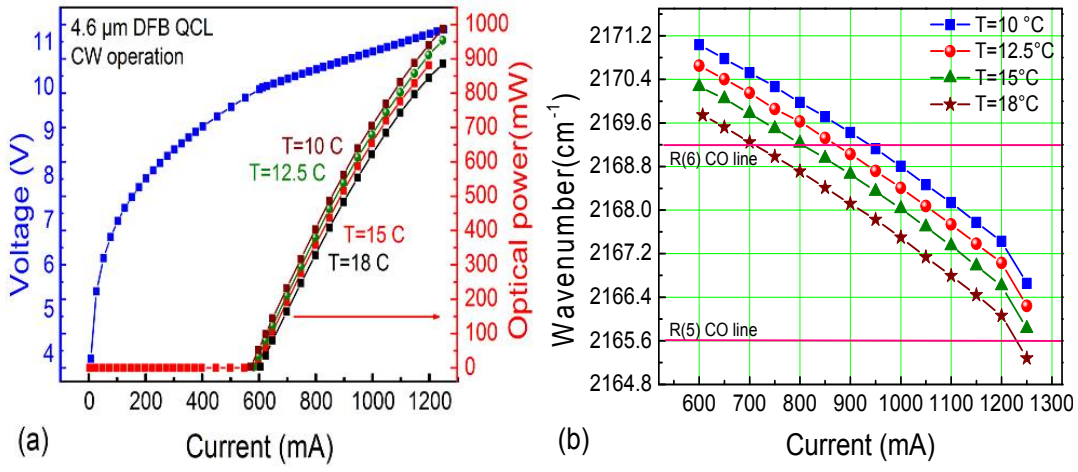

Figure 23.14 (a) LIV curve of the 4.61-µm, RT, CW, DFB-QCL from Center for Quantum Devices, Northwestern University. (b) DFB-QCL current tuning at different DFB-QCL operating temperatures (reprinted from Ref. 9).

For highly accurate and quantitative measurements of carbon monoxide, the R(6) CO absorption line located at 2169.2 cm^{-1} was selected. Based on HITRAN simulation and experimental data, the R(6) CO line is free from spectral interference from CO, N_2O, and H_2O absorption lines and can be measured at atmospheric pressure (760 Torr) using the WMS technique. For N_2O concentration measurements, an interference-free P(41) N_2O absorption line located at 2169.6 cm^{-1} was selected at a gas pressure of 100 Torr. For the CW DFB-QCL operating at 10 °C, the optical power measured after the ADM was 400 mW near 2169 cm^{-1}. High optical power helps to improve the QEPAS signal, which is proportional to $S_0 \sim (\alpha \cdot P \cdot Q)/f_0$, where α is the absorption coefficient, P is the optical power, Q is the quality factor of the resonator, and f_0 is the resonant frequency.

23.4.3.2. Experimental results and discussion

The QEPAS-based sensor performance was tested in two operational modes. In the scanning mode, a small amplitude modulation signal at $f_0/2$ frequency was embedded on top of the slowly changing DC current ramp and added to the DC DFB-QCL current offset, resulting in mode-hop-free frequency tuning over the targeted absorption line. In the line-locking mode, the DFB-QCL frequency was set to the center of the absorption line and actively controlled by the feedback signal of the internal CEU proportional controller based on the 3f component from the pyroelectric detector output [see Fig. 23.11(a) as example]. The proportional controller signal compensates for any laser frequency drift by generating a correction signal to maintain the frequency always at the center of the targeted absorption line.

For the current CO sensor platform based on the NO design described in Section 23.4.2, the maximum 2f QEPAS signal level of the R(6) CO absorption line is obtained at 600 Torr and with a modulation depth of 50 mA. For the same modulation depth, the QEPAS signal value at a pressure of 760 Torr is only ~ 10% lower as compared with the maximum CO signal. However, from a practical point of view, the QEPAS sensor is operated at atmospheric pressure because in this case the pressure controller and flow meter become redundant.

Similar to the NO QEPAS system, the CO signal amplitude signal is strongly dependent on the V-T relaxation rate. Hence, the addition of water vapor to the analyzed gas mixture helps to improve the energy transfer for the V-T states of the excited CO molecules. Therefore, water vapor at different concentration levels was added into the CO:N_2 gas mixture by means of a commercial permeation tube (Perma Pure model MH-110-24F-4), which was immersed inside a water-circulating bath (LAUDA-Brinkmann, LP., RM6). The dependence of the QEPAS signal as a function of the H_2O concentration is shown in Fig. 23.15. The addition of 2.6 % H_2O results in an 8× improvement of the signal amplitude compared with a dry CO:N_2 gas mixture. The insert (a) to Fig. 23.15 shows a difference between the WMS 2f signals for a dry and moisturized (after the addition of 2.6% H_2O concentration) 5-ppmv CO:N_2 mixture. The insert (b) to Fig. 23.15 depicts the background signal measured when the ADM was flushed with ultrahigh-purity N_2. This background signal is primarily determined by fundamental thermal noise of the QTF and is not affected by any optical noise related to the laser beam passing through the ADM. Based on the data depicted in Fig. 23.15, a 1σ MDC limit of the DFB-QCL-based QEPAS CO sensor is 1.5 ppbv for a 1-s data acquisition time. The corresponding normalized noise-equivalent absorption (NNEA) coefficient is 1.61×10^{-8} $cm^{-1}W/\sqrt{Hz}$. The NNEA coefficient was calculated from the following equation: $NNEA = \alpha_{min} \cdot P_0/\sqrt{\Delta f}$, where α_{min} is the minimum detectable absorption coefficient for SNR = 1, P_0 is the optical power, and $\sqrt{\Delta f}$ is the detection bandwidth.

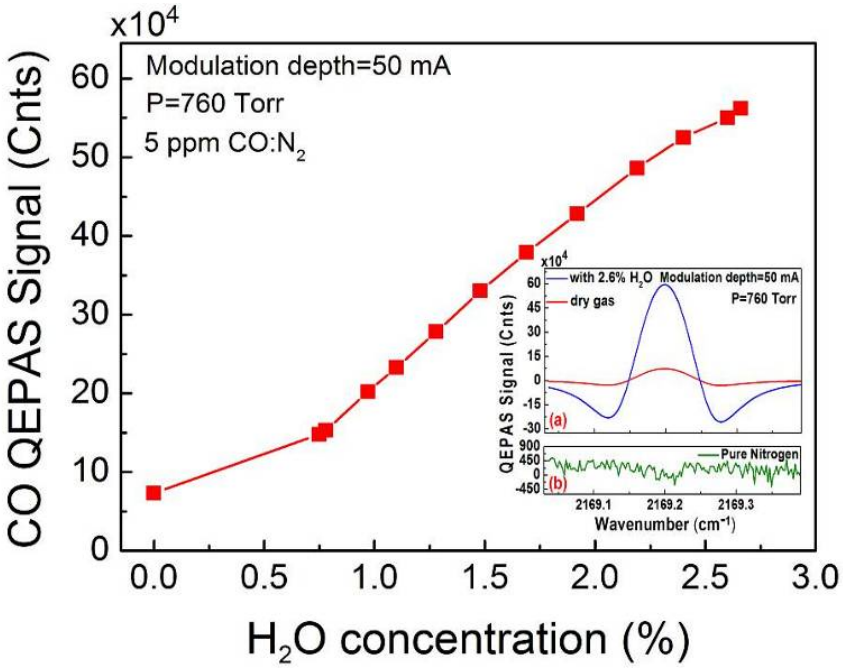

Figure 23.15 Measured QEPAS-based CO signal amplitude as a function of water vapor concentration at atmospheric pressure and a modulation depth of 50 mA. 1 cnt = 6.67×10^{-16} A. Inset (a) QEPAS signal for a 5-ppmv CO:N_2 mixture: dry, and moisturized with 2.6 % H_2O concentration. Inset (b) QEPAS signal for pure N_2 (reprinted from Ref. 9).

Similar measurements were carried out for N_2O detection by targeting the P(41) N_2O absorption line. A certified mixture of 1.8-ppmv N_2O:N_2 was used to evaluate the QEPAS sensor performance in this case. The optimum signal level was obtained when the gas pressure and modulation depth were set to 100 Torr and 20 mA, respectively. The addition of a 2.6% H_2O concentration to the analyzed N_2O:N_2 mixture resulted in a 5-fold enhancement of QEPAS signal amplitude, which resulted in a MDC level of 23 ppbv. The corresponding NNEA coefficient was found to be 2.91×10^{-9} $cm^{-1}W/\sqrt{Hz}$. The N_2O concentration level in laboratory was measured to be 350 ppbv when the QEPAS sensor was operated in the scanning mode.

Continuous monitoring of CO and N_2O concentration levels and the evaluation of the long-term sensor performance of the QEPAS-based sensor system were performed in the line-locking mode, where the CW DFB-QCL frequency is kept at the center of the targeted absorption line. For line-locked measurements of the CO concentration at atmospheric pressure, the modulation depth was decreased from 50 mA to 40 mA because the 3*f* reference signal shape for the QEPAS sensor operating at 760 Torr was pressure broadened. The sealed CO reference cell was filled at a total pressure of 150 Torr.

To verify the linear response of the mid-infrared QEPAS-based CO sensor platform, the calibration mixture of 5-ppm CO:N_2 containing a constant 2.6% concentration of water vapor was diluted 6 times down to 50-ppb CO concentration levels [Fig. 23.16(a)]. The data acquisition times for these measurements were set to 1 s. The measured QEPAS signal amplitude as a function of CO concentration is plotted in the Fig. 23.16(b). The calculated R-square value, which represents how well the regression line approximates real data points, is ~ 0.999 after a

linear fitting procedure. This implies that the sensor system exhibits a good linearity response to monitored CO concentration levels. However, due to the decrease of the modulation depth to 40 mA, the measured signal amplitude of the moisturized 5-ppm CO:N_2 mixture is 22% lower compared to the line-scanning-mode experiments, where a 50-mA modulation depth was used. Based on the data in Fig. 23.16(a), the calculated MDC level is 1.9 ppbv, which is still in good agreement with the MDC value that was previously calculated for the QEPAS sensor operated in the scanning mode. The recalculated NNEA coefficient in this case is 2.04×10^{-8} $cm^{-1}W/\sqrt{Hz}$.

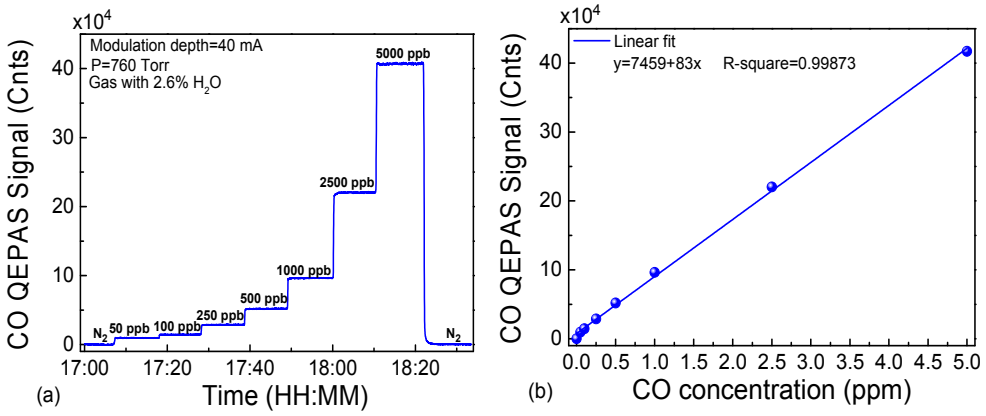

Figure 23.16(a) QEPAS signal amplitude recorded in the line-locking mode as the CO concentration is varied at atmospheric pressure and with a modulation depth of 40 mA. (b) QEPAS signals amplitude averaged from (a) as a function of CO concentration. 1 cnt = 6.67×10^{-16} A (reprinted from Ref. 9).

To investigate the long-term stability and precision of the CO QEPAS sensor, an Allan deviation analysis was also performed while ultrapure nitrogen was flushed through the QEPAS sensor system. Obtained from the Allan deviation plot, the optimum averaging time for the CO sensor is found to be 500 s, which results in a MDC of 280 pptv. For the N_2O QEPAS sensor, when the laser wavelength was locked to the P(41) N_2O line, an Allan deviation analysis shows that, after averaging, acquired data for 500 s the MDL is improved to 4 ppbv.

For ambient CO and N_2O concentration measurements, an inlet tube of the QEPAS sensor was placed outside the laboratory, and the atmospheric air was pumped into the sensor. The results of continuous measurements of atmospheric CO and N_2O concentration levels for a five-hour period are shown in Figs. 23.17(a) and (b), respectively. The highest CO concentration spikes are caused by cigarette smoke, whereas all other less intense spikes, recorded on top of the CO atmospheric background of ~130 ppbv, are due to automobile emissions. The mean atmospheric concentration of N_2O was calculated to be 350 ppbv when using the P(41) N_2O line at 2169.6 cm^{-1}. Due to a long atmospheric residence time, the N_2O concentration is well mixed in the lower atmosphere; therefore, its atmospheric concentration level is relatively stable, as can be seen from Fig. 23.17(b). The continuous monitoring of atmospheric CO and N_2O concentration levels for more than five hours indicated the stability and robustness of the reported DFB-QCL-based QEPAS sensor system.

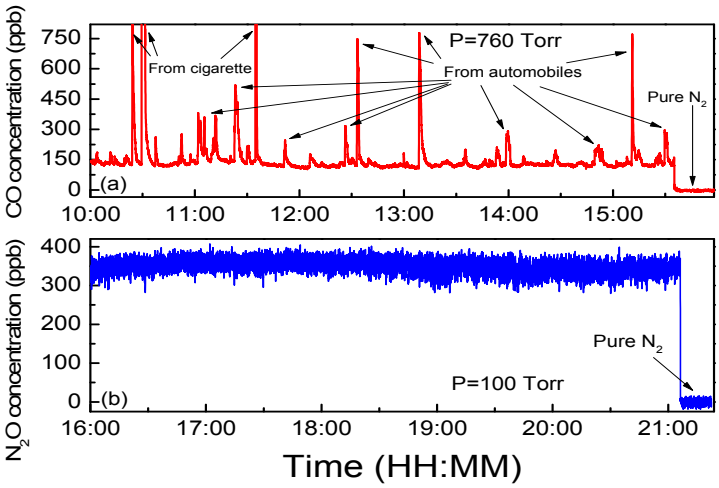

Figure 23.17 Continuous monitoring of atmospheric CO and N_2O concentration levels from an air sampled on Rice University campus, Houston, TX , USA (latitude and longitude are: 29 deg 43' N/95 deg 23' W). (a) CO concentration measurements. (b) N_2O concentration measurements (reprinted from Ref. 9).

23.4.4 Sulfur dioxide experiments

The QEPAS sensor technique was also employed for detecting and monitoring sulfur dioxide (SO_2) at ppbv-concentration levels with a time response of 1 s, suitable for environmental monitoring, industrial processing, and noninvasive exhaled breath analysis. SO_2 is a major air pollutant and has significant impact on human health by affecting lungs and causing breathing difficulties. The major sources of SO_2 emission into the atmosphere are associated with industrial combustion processes as well as automobile, truck, aircraft and marine transport emissions. SO_2 becomes toxic when its concentration exceeds 1 ppmv in ambient air.[55]

23.4.4.1 SO_2 QEPAS sensor architecture and performance

In this work, the QEPAS-based chemical sensing platform [similar to that depicted in Fig. 23.11(a)] consists of a 7.25-μm CW DFB-QCL in an HHL package, an aspheric black-diamond lens (f = 4 mm) to collimate the emitted laser beam, two planoconvex germanium lenses (f = 25 mm) with broadband AR coatings, and a 150-μm pinhole used as a spatial filter. A single-frequency DFB-QCL current tuning and optical power values at four different operating temperatures are demonstrated in Fig. 23.18(a) and (b), respectively.

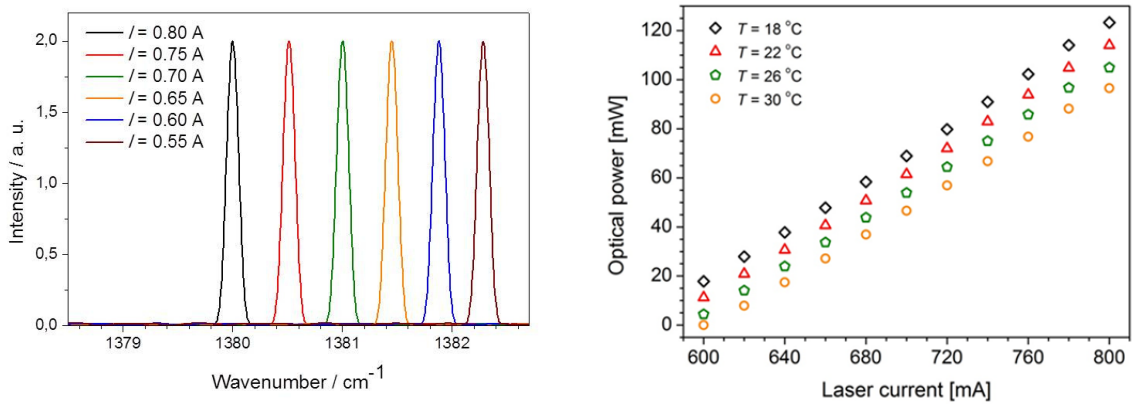

(a) (b)

Figure 23.18 (a) Single-frequency CW DFB-QCL radiation for different laser current values at a QCL-operating temperature of 20 °C. (b) CW DFB-QCL optical power and current tuning at four different operating temperatures (reprinted from Ref. 9).

To perform spectroscopic measurements, the DFB-QCL temperature was fixed at 20.5 °C, and emission wavelength was tuned across the SO_2 absorption line centered at 1380.94 cm^{-1}. The sensitivity and linearity of the QEPAS-based SO_2 sensor was investigated in the laser-scanning-mode operation by diluting the wet (2.4% of the water vapor) certified mixture of 10-ppm SO_2 in N_2 to the level of 5, 2, 1, and 0.1 ppm, and by measuring amplitudes of each QEPAS signal respectively. After adding water vapor to the analyzed SO_2 mixture, a more than 3× improvement in detected signal was observed. The measured 2*f* WMS signals corresponding to different SO_2 concentration levels and the linearity plot of the QEPAS sensor are demonstrated in Fig. 23.19 and its inset. The noise level was determined from the baseline recorded with the gas cell filled with ambient air. The minimum detectable SO_2 concentration level (1σ) was calculated to be 100 ppb for the lock-in amplifier time constant set to 1 s. In order to distinguish single absorption lines from the congested spectrum of the SO_2, the pressure inside the ADM was kept at 100 Torr.

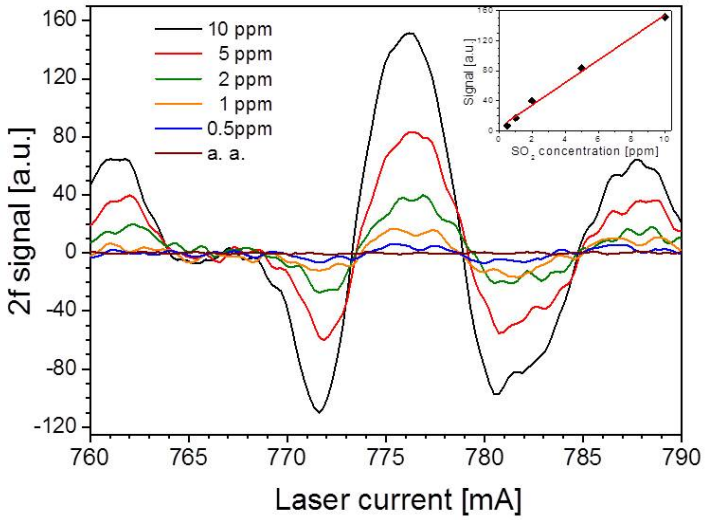

Figure 23.19 2*f* WM QEPAS signals for different SO_2 concentrations when the laser was tuned across the 1380.9 cm^{-1} line. a.a – ambient air. Inset: Dependence of the measured 2*f* signals as a function of SO_2 concentrations (reprinted from Ref. 9).

Future tasks for SO_2 detection will include line locking for continuous and long-term measurements as well as using a high-power (> 200 mW) QCL targeting the strongest SO_2 absorption line at 1348 cm^{-1}. In this situation, a SO_2 detection limit can be improved to low ppb levels; therefore, QEPAS sensors will have the potential to be used as a compact, portable, analytical devices to perform real-time environmental and industrial emission measurements of SO_2.

23.5 Conclusions

This chapter described autonomously operated, compact, reliable, and real-time gas sensors and demonstrated their potential as practical monitoring devices in atmospheric chemistry, and urban and rural environmental monitoring as well as in industrial emission and manufacturing control processes. These sensors can also be used in biomedical and life sciences, such as for noninvasive medical diagnostics that involves the detection and monitoring of numerous exhaled breath biomarkers, and for sensing of trace-gas species relevant to spacecraft habitat air quality and safety or planetary atmospheric science. Several examples of ultrasensitive and selective sensors, with detection limits at ppb and sub-ppb levels, are reported here using mid-infrared CW DFB diode laser EC-QCL and DFB-QCL excitation sources. Details of three spectroscopic techniques that included TDLAS, CPAS, and QEPAS were discussed. The choice of a specific spectroscopic measurement method was determined by the application as well as the readily commercial availability of the appropriate mid-infrared laser source. For example, to detect C_2H_6, a 3.36-μm CW TEC TO5 packaged diode-laser-based TDLAS sensor system with a 1σ C_2H_6 detection sensitivity of 130 pptv (1-s sampling time) was employed. For environmental NH_3 detection, a 1σ NH_3 detection sensitivity of ~ 1 ppbv (200-s averaging time) was reported for a 10.36-μm Daylight Solutions EC-QCL-based CPAS sensor. To monitor CH_4 and N_2O, NO, CO, and SO_2 concentration levels, four different QEPAS-based sensors based on a DFB-QCL from AdtechOptics (7.28 μm), Maxion Technologies (5.26 μm), Northwestern University (4.61 μm), and Hamamatsu (7.24 μm) were employed, respectively. Detection sensitivities for these five gas species were 20 ppbv, 7 ppbv, 3 ppbv, 2 ppbv and 100 ppbv, respectively for a 1-s sampling time. Improvements and innovations in TDLAS-, CPAS-, and QEPAS-based sensor platforms (in particular more stable, mass-produced optical/mechanical designs as well as data acquisition and noise reduction techniques) will lead to near- or mid-infrared laser-based optical instruments that can be operated by nontechnical personnel and be manufactured at sufficiently low cost, leading to sensor networks that permit both temporal and spatial trace-gas monitoring.

Seventeen trace-gas species that have been detected to date with QEPAS sensor technology at Rice University are listed in Table 23.1. The highest NNEA coefficient value measured to date using QEPAS is 1.9×10^{-9} $cm^{-1}W/\sqrt{Hz}$.[56] Most of the listed molecules have an NNEA coefficient (fourth column of the table) comparable to the NNEA value of the conventional PAS technique (2.2×10^{-9} $cm^{-1}W/\sqrt{Hz}$).[57] Molecules shown in this table were detected based on near-infrared semiconductor diode laser sensors (green section), and interband cascade (IC) or quantum cascade (QC) laser sensors (dark yellow section), respectively.

Molecule (host)	Frequency (cm^{-1})	Pressure (Torr)	NNEA ($cm^{-1}W/Hz^{1/2}$)	Power (mW)	NEC (ppmv)
H_2O (N_2)**	7306.75	60	1.9×10^{-9}	9.5	0.09
HCN (air: 50% RH)*	6539.11	60	4.6×10^{-9}	50	0.16
C_2H_2 (N_2)*	6523.88	720	4.1×10^{-9}	57	0.03
NH_3 (N_2)*	6528.76	575	3.1×10^{-9}	60	0.06
C_2H_4 (N_2)*	6177.07	715	5.4×10^{-9}	15	1.7
CH_4 (N_2+1.2%H_2O)*	6057.09	760	3.7×10^{-9}	16	0.24
CO_2 (breath ~ 50% RH)	6361.25	150	8.2×10^{-9}	45	40
H_2S (N_2)*	6357.63	780	5.6×10^{-9}	45	5
HCl (N_2 dry)	5739.26	760	5.2×10^{-8}	15	0.7
CO_2 (N_2 + 1.2%H_2O)*	4991.26	50	1.4×10^{-8}	4.4	18
CH_2O (N_2: 75% RH)*	2804.90	75	8.7×10^{-9}	7.2	0.12
CO (N_2 + 2.2% H_2O)*	2176.28	100	1.4×10^{-7}	71	0.002
NO (N_2 + H_2O)	1900.07	250	7.5×10^{-9}	100	0.003
C_2H_5OH (N_2)**	1934.2	770	2.2×10^{-7}	10	90
SO_2 (N_2 + 2.4% H_2O)*	1380.94	100	2.0×10^{-8}	40	0.1
N_2O (air)	1275.492	230	5.3×10^{-8}	123	0.007
CH_4 (air)	1275.386	230	1.7×10^{-7}	158	0.02
C_2HF_5 (N_2)***	1208.62	770	7.8×10^{-9}	6.6	0.009
NH_3 (N_2)*	1046.39	110	1.6×10^{-8}	20	0.006

Table 23.1 Near-IR laser diode and mid-IR-QCL-based QEPAS performance for 17 trace gas species. RH – relative humidity.

* Improved microresonator.
** Improved microresonator and double optical pass through ADM.

*** With amplitude modulation and metal microresonator (NNEA coefficient; NEC for available laser power and τ = 1-s time constant, 18 dB/oct. filter slope).

Improvements of existing sensing technologies, especially based on photoacoustic spectroscopy, can be achieved by using novel, thermoelectrically cooled, room-temperature-operated, high-performance mid-infrared QCLs. The development of narrow-linewidth QCLs is rapidly progressing, and QC lasers with an internal grating producing ~ 1 W of CW power are already technically feasible.[58,59] With significant advances in single-frequency EC-QCL and DFB-QCL technology, it is expected that further progress in their application in laser-based spectroscopic measurements will be achieved.

Acknowledgements

The Rice University group acknowledges financial support from a National Science Foundation (NSF) grant EEC-0540832 entitled "Mid-Infrared Technologies for Health and the Environment (MIRTHE)," an NSF-ANR award for international collaboration in chemistry: "Next generation of compact infrared laser-based sensor for environmental monitoring (NexCILAS)" and grant C-0586 from the Robert Welch Foundation.

References

1. J. Faist, F. Capasso, D. L. Sivco, A. L. Hutchinson, and A. Y. Cho, "Quantum cascade laser," *Science* **264**, 553–556 (1994); J. Faist, *Quantum Cascade Lasers*, Oxford University Press, Oxford (2013).
2. F. Capasso, "High-performance mid-infrared quantum cascade lasers," *Opt. Eng.* **49**(11), 111102 (2010) [doi: 10.1117/1.3505844].
3. R. Q. Yang, "Infrared laser based on intersubband transitions in quantum wells," *Superlattices and Microstructures* **17**, 77–83 (1995).
4. J. R. Meyer, I. Vurgaftman, R. Q. Yang, and L. R. Ram-Mohan, "Type-II and type-I interband cascade lasers," *Electron. Lett.* **32**, 45–46 (1996).
5. K. Krzempek, R. Lewicki, L. Nähle, M. Fischer, J. Koeth, S. Belahsene, Y. Rouillard, L. Worschech, and F. K. Tittel, "Continuous wave, distributed feedback diode laser based sensor for trace-gas detection of ethane," *Appl. Phys. B* **106**, 251–255 (2012).
6. A. Kosterev, L. Dong, D. Thomazy, F. Tittel, and S. Overby, "QEPAS for chemical analysis of multi-component gas mixtures," *Appl. Phys. B: Lasers and Optics* **101**, 649–659 (2010).
7. M. Jahjah, S. Belahsene, L. Nähle, M. Fischer, J. Koeth, Y. Rouillard, and A. Vicet, "Quartz enhanced photoacoustic spectroscopy with a 3.38 μm antimonide distributed feedback laser," *Opt. Lett.* **37**, 2502–2504 (2012).
8. L. Dong, R. Lewicki, R. J. Griffin, J. H. Flynn, B. L. Lefer, and F. K. Tittel, "Atmospheric ammonia measurements in Houston, TX using an external-cavity quantum cascade laser-based sensor," *Atmos. Chem. Phys.* **11**, 97219733 (2011).
9. R. Lewicki, L. Dong, Y. Ma, and F. K. Tittel, "A compact CW quantum cascade laser based QEPAS sensor for sensitive detection of nitric oxide," paper presented at the CLEO 2012 Conf. on Lasers and Electro-Optics (2012).

10. L. Dong, V. Spagnolo, R. Lewicki, and F. K. Tittel, "Ppb-level detection of nitric oxide using an external cavity quantum cascade laser based QEPAS sensor," *Opt. Express* **19**, 24037–24045 (2011).

11. Y. Ma, R. Lewicki, M. Razeghi, and F. K. Tittel, "QEPAS based ppb-level detection of CO and N_2O using a high power CW DFB-QCL," *Opt. Express* **21**, 1008–1019 (2013).

12. J. Waclawek, R. Lewicki, M. Jahjah, Y. Ma, E. Chrysostom, B. Lendl, and F. K. Tittel, "A sensitive CW DFB quantum cascade laser based QEPAS sensor for detection of SO_2," paper presented at the CLEO 2012 Conf. on Lasers and Electro-Optics (2012).

13. A. A. Kosterev, Y. A. Bakhirkin, R. F. Curl, and F. K. Tittel, "Quartz-enhanced photoacoustic spectroscopy," *Opt. Lett.* **27**, 1902–1904 (2002).

14. A. Kosterev, G. Wysocki, Y. Bakhirkin, S. So, R. Lewicki, M. Fraser, F. Tittel, and R. F. Curl, "Application of quantum cascade lasers to trace gas analysis," *Appl. Phys. B: Lasers and Optics* **90**, 165–176 (2008).

15. M. Jahjah, A. Vicet, and Y. Rouillard, "A QEPAS based methane sensor with a 2.35 μm antimonide laser," *Appl. Phys. B* **106**, 483–489 (2012).

16. R. F. Curl, F. Capasso, C. Gmachl, A. A. Kosterev, B. McManus, R. Lewicki, M. Pusharsky, G. Wysocki, F. K. Tittel, "Quantum cascade lasers in chemical physics," *Chem. Phys. Lett.* **487**, 1–18 (2010).

17. D. M. Sonnenfroh, W. T. Rawlins, M. G. Allen, C. Gmachl, F. Capasso, A. L. Hutchinson, D. L. Sivco, J. N. Baillargeon, and A. Y. Cho, "Application of balanced detection to absorption measurements of trace gases with room-temperature, quasi-cw quantum-cascade lasers," *Appl. Opt.* **40**, 812–820 (2001).

18. E. G. Snyder, C. A. Munson, J. L. Gottfried, J. F. C. De Lucia, B. Gullett, and A. Miziolek, "Laser-induced breakdown spectroscopy for the classification of unknown powders," *Appl. Opt.* **47**, G80–G87 (2008).

19. J. Gottfried, F. Lucia, Jr., C. Munson, and A. Miziolek, "Laser-induced breakdown spectroscopy for detection of explosives residues: A review of recent advances, challenges, and future prospects," *Anal. Bioanal. Chem.* **395**, 283–300 (2009).

20. J. Ye, L.-S. Ma, and J. L. Hall, "Ultrasensitive detections in atomic and molecular physics: Demonstration in molecular overtone spectroscopy," *J. Opt. Soc. Am. B* **15**, 6–15 (1998).

21. A. Foltynowicz, W. Ma, and O. Axner, "Characterization of fiber-laser-based sub-Doppler NICE-OHMS for quantitative trace gas detection," *Opt. Express* **16**, 14689–14702 (2008).

22. G. Litfin, C. R. Pollock, R. F. Curl, and F. K. Tittel, "Sensitivity enhancement of laser absorption spectroscopy by magnetic rotation effect," *J. Chem. Phys.* **72**, 6602–6605 (1980).

23. H. Ganser, W. Urban, and A. M. Brown, "The sensitive detection of NO by Faraday modulation spectroscopy with a quantum cascade laser," *Molec. Phys.* **101**, 545–550 (2003).

24. R. Lewicki, J. H. Doty, R. F. Curl, F. K. Tittel, and G. Wysocki, "Ultrasensitive detection of nitric oxide at 5.33 μm by using external cavity quantum cascade laser-based Faraday rotation spectroscopy," *Proc. Natl. Acad. Sci. USA* **106**, 12587–12592 (2009).

25. M. J. Thorpe, D. D. Hudson, K. D. Moll, J. Lasri, and J. Ye, "Cavity-ringdown molecular spectroscopy based on an optical frequency comb at 1.45-1.65 μm," *Opt. Lett.* **32**, 307–309 (2007).

26. M. J. Thorpe, D. Balslev-Clausen, M. S. Kirchner, and J. Ye, "Cavity-enhanced optical frequency comb spectroscopy: Application to human breath analysis," *Opt. Express* **16**, 2387–2397 (2008).

27. B. Hirst, G. Gibson, S. Gillespie, I. Archibald, O. Podlaha, K. D. Skeldon, J. Courtial, S. Monk, and M. Padgett, "Oil and gas prospecting by ultra-sensitive optical gas detection with inverse gas dispersion modelling," *Geophys. Res. Lett.* **31**, L12115 (2004).

28. C. Wang and P. Sahay, "Breath analysis using laser spectroscopic techniques: Breath biomarkers, spectral fingerprints, and detection limits," *Sensors* **9**, 8230–8262 (2009).

29. A. Bari, V. Ferraro, L. R. Wilson, D. Luttinger, and L. Husain, "Measurements of gaseous HONO, HNO_3, SO_2, HCl, NH_3, particulate sulfate and PM2.5 in New York, NY," *Atmospheric Environment* **37**, 2825–2835 (2003).

30. A. Rossi, R. Buffa, M. Scotoni, D. Bassi, S. Iannotta, and A. Boschetti, "Optical enhancement of diode laser-photoacoustic trace gas detection by means of external Fabry-Perot cavity," *Appl. Phys. Lett.* **87**, 041110 (2005).

31. A. Miklos, P. Hess, and Z. Bozoki, "Application of acoustic resonators in photoacoustic trace gas analysis and metrology," *Rev. Sci. Instrum.* **72**, 1937–1955 (2001).

32. D. Hofstetter, M. Beck, J. Faist, M. Nägele, and M. W. Sigrist, "Photoacoustic spectroscopy with quantum cascade distributed-feedback lasers," *Opt. Lett.* **26**, 887–889 (2001).

33. M. G. da Silva, H. Vargas, A. Miklós, and P. Hess, "Photoacoustic detection of ozone using a quantum cascade laser," *Appl. Phys. B: Lasers and Optics* **78**, 677–680 (2004).

34. M. Pushkarsky, A. Tsekoun, I. G. Dunayevskiy, R. Go, and C. K. N. Patel, "Sub-parts-per-billion level detection of NO_2 using room-temperature quantum cascade lasers," *Proc. Natl. Acad. Sci. USA* **103**, 10846–10849 (2006).

35. J. P. Lima, H. Vargas, A. Miklós, M. Angelmahr, and P. Hess, "Photoacoustic detection of NO_2 and N_2O using quantum cascade lasers," *Appl. Phys. B: Lasers and Optics* **85**, 279–284 (2006).

36. A. A. Kosterev, F. K. Tittel, D. V. Serebryakov, A. L. Malinovsky, and I. V. Morozov, "Applications of quartz tuning forks in spectroscopic gas sensing," *Rev. Sci. Instrum.* **76**, 43105–43105 (2005).

37. L. Dong, J. Wright, B. Peters, B. A. Ferguson, F. K. Tittel, and S. McWhorter, "Compact QEPAS sensor for trace methane and ammonia detection in impure hydrogen," *Appl. Phys. B* **107**, 459–467 (2012).

38. R. Lewicki, G. Wysocki, A. A. Kosterev, and F. K. Tittel, "Carbon dioxide and ammonia detection using 2 μm diode laser based quartz-enhanced photoacoustic spectroscopy," *Appl. Phys. B: Lasers and Optics* **87**, 157–162 (2007).

39. L. Dong, A. Kosterev, D. Thomazy, and F. Tittel, "QEPAS spectrophones: Design, optimization, and performance," *Appl. Phys. B: Lasers and Optics* **100**, 627–635 (2010).

40. K. Liu, X. Y. Guo, H. M. Yi, W. D. Chen, W. J. Zhang, X. M. Gao, "Off-beam quartz-enhanced photoacoustic spectroscopy," *Opt. Lett.* **34**, 1594–1596 (2009).

41. K. Liu, H. Yi, A. A. Kosterev, W. Chen, L. Dong, L. Wang, T. Tan, W. Zhang, F. K. Tittel, and X. Gao, "Trace gas detection based on off-beam quartz enhanced photoacoustic spectroscopy: Optimization and performance evaluation," *Rev. Sci. Instrum.* **81**, 103103 (2010).

42. M. Köhring, A. Pohlkötter, U. Willer, M. Angelmahr, and W. Schade, "Tuning fork enhanced interferometric photoacoustic spectroscopy: A new method for trace gas analysis," *Appl. Phys. B* **102**, 133–139 (2011).

43. A. A. Kosterev and J. H. Doty III, "Resonant optothermoacoustic detection: technique for measuring weak optical absorption by gases and micro-objects," *Opt. Lett.* **35**, 3571–3573 (2010).

44. P. Kluczynski, S. Lundqvist, S. Belahsene, and Y. Rouillard, "Tunable-diode-laser spectroscopy of C_2H_2 using a 3.03 μm GaInAsSb/AlGaInAsSb distributed-feedback laser," *Opt. Lett.* **34**, 3767–3769 (2009).

45. L. Nähle, S. Belahsene, M. von Edlinger, M. Fischer, G. Boissier, P. Grech, G. Narcy, A. Vicet, Y. Rouillard, J. Koeth, and L. Worschech, "Continuous-wave operation of type-I quantum well DFB laser diodes emitting in 3.4 μm wavelength range around room temperature," *Electron. Lett.* **47**, 46–47 (2011).

46. D. Herriott, H. Kogelnik, and R. Kompfner, "Off-axis paths in spherical mirror interferometers," *Appl. Opt.* **3**, 523–526 (1964).

47. D. R. Herriott and H. J. Schulte, "Folded optical delay lines," *Appl. Opt.* **4**, 883 (1965).

48. F. J. Dentener and P. J. Crutzen, "A three-dimensional model of the global ammonia cycle," *J. Atmosph. Chem.* **19**, 331–369 (1994).

49. C.-M. Lee, K. V. Bychkov, V. A. Kapitanov, A. I. Karapuzikov, Y. N. Ponomarev, I. V. Sherstov, and V. A. Vasiliev, "High-sensitivity laser photoacoustic leak detector," *Opt. Eng.* **46**, 064302 (2007) [doi: 10.1117/1.2748042].

50. J. Seinfeld and S. Pandis, *Atmospheric Chemistry and Physics: From Air Pollution to Climate Change*, Wiley & Sons, New York (1998).

51. T. Risby and F. K. Tittel, "Current status of mid-infrared quantum and interband cascade lasers for clinical breath analysis," *Opt. Eng.* **49**(11), 111123 (2010) [doi: 10.1117/1.3498768].

52. M. R. McCurdy, A. Sharafkhaneh, H. Abdel-Monem, J. Rojo, and F. K. Tittel, "Exhaled nitric oxide parameters and functional capacity in chronic obstructive pulmonary disease," *J. Breath Res.* **5**, 016003 (2011).

53. S. Schilt, L. Thévenaz, and P. Robert, "Wavelength modulation spectroscopy: Combined frequency and intensity laser modulation," *Appl. Opt.* **42**, 6728–6738 (2003).

54. X. Chao, J. B. Jeffries, and R. K. Hanson, "Wavelength-modulation-spectroscopy for real-time, in situ NO detection in combustion gases with a 5.2 μm quantum-cascade laser," *Appl. Phys. B* **106**, 987–997 (2012).

55. World Bank, *Pollution Prevention and Abatement Handbook, 1998*: *Toward Cleaner Production*, The World Bank Group (1998).

56. A. A. Kosterev, F. K. Tittel, T. S. Knittel, A. Cowie, and J. D. Tate, "Trace humidity sensor based on quartz-enhanced photoacoustic spectroscopy," paper presented at Conf. on Laser Applications to Chemical, Security and Environmental Analysis, Incline Village, Nevada (2006).

57. M. E. Webber, M. Pushkarsky, and C. K. N. Patel, "Fiber-amplifier-enhanced photoacoustic spectroscopy with near-infrared tunable diode lasers," *Appl. Opt.* **42**, 2119–2126 (2003).

58. M. Razeghi, Y. Bai, S. Slivken, and S. R. Darvish, "High-performance InP-based midinfrared quantum cascade lasers at Northwestern University," *Opt. Eng.* **49**, 111103 (2010) [doi: 10.1117/1.3497623].

59. A. Lyakh, R. Maulini, A. G. Tsekoun, and C. K. N. Patel, "Progress in high-performance quantum cascade lasers," *Opt. Eng.* **49**, 111105 (2010) [doi: 10.1117/1.3506192].

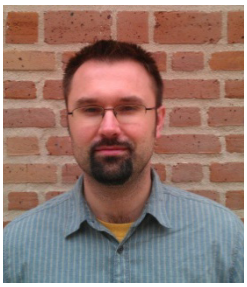

Rafał Lewicki received his M.S. degree and Ph.D. degree (cum laude) in electronics from Wroclaw University of Technology, Wroclaw, Poland in 2005 and 2011, respectively. In December 2005, he joined the Laser Science Group at Rice University, Houston, Texas, as a visiting scholar, and currently he holds a postdoctoral research associate position in the Department of Electrical and Computer Engineering at Rice University. His research interest is focused on trace gas detection using laser-based spectroscopic techniques. He is currently working on the implementation of QCL-based sensor platforms enabling high-resolution, selective, and real time spectroscopic measurements, for applications in environmental monitoring, medical diagnostics, and industrial process control. He has coauthored 16 peer-reviewed journal publications, 4 book chapters, and more than 40 conference presentations in the field of laser spectroscopy.

Mohammad Jahjah was awarded the Ph.D. degree in electronics from Université Montpellier 2, Montpellier, France in 2011 for his work focused on developing an innovative spectroscopic multigas absorption system by using tunable diode lasers emitting in the mid-infrared. In 2012, Mohammad Jahjah joined Laser and Science Group as a postdoctoral research associate at Rice University in Houston, TX, under the supervision of Professor Frank Tittel. Mohammad is currently working on setting up optical sensors based on tunable lasers (QCLs, diode lasers, etc.) for health diagnostics and environmental applications. Mohammad Jahjah has coauthored 8 peer-reviewed journal publications, 2 book chapters, and 10 conference papers in the fields of laser spectroscopy and science and innovations.

Yufei Ma received his Master's degree in physical electronics in 2008 from Harbin Institute of Technology, Harbin, China, and currently is working toward a Ph.D. degree from the same university. In September 2011, he joined Prof. Tittel's group at Rice University, Houston, Texas, as a visiting student for one year. His current research activities include QCLs and quartz-enhanced photoacoustic spectroscopy-based trace gas sensing for environmental applications and solid state laser technologies.

Przemyslaw Stefański received his B.Sc. degree in electronics from Wroclaw University of Technology (Wroclaw, Poland) in 2012. Mr. Stefanski is currently in his second year of the Advanced Applied Electronics program and will receive a M.S. degree in 2013. In July 2012, Mr. Stefanski joined Rice University Laser Science Group (Houston, Texas) as a visiting scholar for one year. His current research interests include trace gas sensing and analysis, as well as the design of analog and microcontroller-based electronic systems. His present work is focused

on the implementation of optical sensor platforms based on different types of mid-infrared lasers, employing various spectroscopic techniques for trace gas sensing.

Jan Tarka received the B.Sc. in electronics in Wroclaw University of Technology, Poland, in 2012. In July 2012 he joined Laser Science Group at Rice University, Houston, Texas as a visiting graduate student. His research work is focused on developing QCL-based trace gas sensor platforms for environmental applications. His current projects are related to ultrasensitive detection of atmospheric species using absorption spectroscopy with a multipass cell and Faraday rotation spectroscopy techniques.

Manijeh Razeghi received the Doctorat d'État ès Sciences Physiques from the Université de Paris, France, in 1980. After heading the Exploratory Materials Lab at Thomson-CSF (France), she joined Northwestern University, Evanston, Illinois, as a Walter P. Murphy Professor and Director of the Center for Quantum Devices in fall 1991, where she created the undergraduate and graduate program in solid state engineering. She is one of the leading scientists in the field of semiconductor science and technology, pioneering in the development and implementation of major modern epitaxial techniques such as MOCVD, VPE, gas MBE, and MOMBE for the growth of entire compositional ranges of III-V compound semiconductors. She is on the editorial board of many journals such as *Journal of Nanotechnology*, and *Journal of Nanoscience and Nanotechnology*, and is an Associate Editor of *Opto-Electronics Review*. She is on the International Advisory Board for the Polish Committee of Science and is an Adjunct Professor at the College of Optical Sciences of the University of Arizona, Tucson, Arizona. She has authored or coauthored more than 1000 papers, more than 30 book chapters, and fifteen books, including the textbooks *Technology of Quantum Devices* (Springer Science+Business Media (2010) and *Fundamentals of Solid State Engineering, 3rd Edition* (Springer Science+Business Media (2009). Two of her books, *MOCVD Challenge Vol. 1* (IOP Publishing Ltd. (1989) and *MOCVD Challenge Vol. 2* (IOP Publishing Ltd. (1995), discuss some of her pioneering work in InP-GaInAsP and GaAs-GaInAsP based systems. *The MOCVD Challenge*, *Second ed*., Taylor & Francis/CRC Press (2010) represents the combined updated version of Volumes 1 and 2. She holds 50 U.S. patents and has given more than 1000 invited and plenary talks. Her current research interest is in nanoscale optoelectronic quantum devices.

Dr. Razeghi is a Fellow of MRS, IOP, IEEE, APS, SPIE, OSA, a Fellow and Life Member of the Society of Women Engineers (SWE), a Fellow of the International Engineering Consortium (IEC), and a member of the Electrochemical Society, ACS, AAAS, and the French Academy of Sciences and Technology. She received the IBM Europe Science and Technology Prize in 1987, the Achievement Award from the SWE in 1995, the R. F. Bunshah Award in 2004, and many best-paper awards.

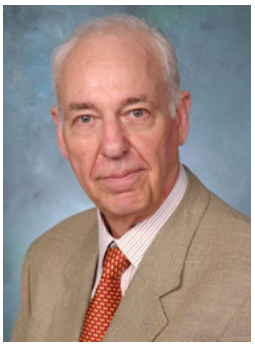

Frank K. Tittel is the J. S. Abercrombie Professor of Electrical & Computer Engineering at Rice University and a joint faculty appointment in the Bioengineering Department. He obtained his B.Sc. and Ph.D. in physics from Oxford University in 1955 and 1959, respectively. From 1959 to 1967 he was a research physicist with General Electric Research & Development Center, Schenectady, New York. Since 1967, he has been on the faculty at Rice University. Current research interests include various aspects of quantum electronics, specifically laser spectroscopy and laser applications in environmental monitoring, industrial process control, and medicine. He has published more than 370 technical papers and holds 9 U.S. patents in these areas. Dr. Tittel is a Fellow of the IEEE, the Optical Society of America, and the American Physical Society. He received a Doctor of Science degree from Szeged University in 1993 and an honorary Professor appointment from Harbin Institute of Technology in 1986.